AD-A035 678

SUPERSONIC CHORDWISE BENDING FLUTTER IN CASCADES

PRATT AND WHITNEY AIRCRAFT
EAST HARTFORD, CONNECTICUT

31 MAY 1975

Report No. PWA-5271

SUPERSONIC CHORDWISE BENDING FLUTTER IN CASCADES

R. A. Arnoldi, F. O. Carta
A. O. St. Hilaire and W. N. Dalton III

Pratt & Whitney Aircraft
Division of United Technologies Corporation
East Hartford, Connecticut

31 May 1975

Final Technical Report
(1 April 1974 to 31 May 1975)

This report is not releasable to foreign nationals or to personnel possessing "Reciprocal" clearances without the written approval of NAVAIR (AIR-802).

Prepared Under Contract N00019-74-C-0305

for

Naval Air Systems Command
Washington, D. C. 20361

Report No. PWA-5271

SUPERSONIC CHORDWISE BENDING FLUTTER IN CASCADES

R. A. Arnoldi, F. O. Carta
A. O. St. Hilaire and W. N. Dalton III

Pratt & Whitney Aircraft
Division of United Technologies Corporation
East Hartford, Connecticut

31 May 1975

Final Technical Report
(1 April 1974 to 31 May 1975)

This report is not releasable to foreign nationals or to personnel possessing "Reciprocal" clearances without the written approval of NAVAIR (AIR-532).

Prepared Under Contract N00019-74-C-0305

for

Naval Air Systems Command
Washington, D. C. 20361

APPROVED FOR PUBLIC RELEASE:
DISTRIBUTION UNLIMITED

REPORT DOCUMENTATION PAGE

READ INSTRUCTIONS BEFORE COMPLETING FORM

1 REPORT NUMBER: PWA-5271	2 GOVT ACCESSION NO.
3 RECIPIENT'S CATALOG NUMBER	
4. TITLE (and Subtitle): Supersonic Chordwise Bending Flutter in Cascade	5 TYPE OF REPORT & PERIOD COVERED: Final Technical Report (1 April 1974 to 31 May 1975)
6 PERFORMING ORG. REPORT NUMBER	
7. AUTHOR(s): R. A. Arnoldi, F. O. Carta, A. O. St. Hilaire and W. N. Dalton III	8 CONTRACT OR GRANT NUMBER(s): N00019-74-C-0305
9. PERFORMING ORGANIZATION NAME AND ADDRESS: Pratt & Whitney Aircraft Division, United Technologies Corporation, East Hartford, Conn. 06108	10 PROGRAM ELEMENT, PROJECT, TASK AREA & WORK UNIT NUMBERS: 310A-014-4
11. CONTROLLING OFFICE NAME AND ADDRESS: Naval Air Systems Command, Department of the Navy, Washington, D. C. 20360	12 REPORT DATE: 31 May 1975
	13 NUMBER OF PAGES
14 MONITORING AGENCY NAME & ADDRESS (if different from Controlling Office)	15 SECURITY CLASS (of this report): UNCLASSIFIED
	15a DECLASSIFICATION/DOWNGRADING SCHEDULE

16 DISTRIBUTION STATEMENT (of this Report)

This report is not releasable to foreign nationals or to persons possessing "Reciprocal" clearances without the written approval of NAVAIR (AIR-602).

APPROVED FOR PUBLIC RELEASE: DISTRIBUTION UNLIMITED

17 DISTRIBUTION STATEMENT (of the abstract entered in Block 20, if different from Report)

18 SUPPLEMENTARY NOTES

19 KEY WORDS (Continue on reverse side if necessary and identify by block number)

Flutter, Unsteady Aerodynamics, Gas Turbine Engines, Mechanical Vibrations.

20 ABSTRACT (Continue on reverse side if necessary and identify by block number)

This report documents the results of an experimental program to study the phenomenon of chordwise bending flutter. An extensive series of vibration bench tests, using both prototype blades and the actual J-blade hardware, resulted in the choice of the first bending mode of a fully double-cantilevered configuration as the chordwise bending mode to be tested. Alterations in both method of blade attachment and in the blade geometry itself were introduced to improve the desired mode shape and frequency. The vibration bench tests were carried out in conjunction with NASTRAN predictions and supersonic cascade aerodynamic computations. Comparisons between theory and experiment are discussed.

20. ABSTRACT (Cont'd)

Two blade configurations were flutter tested. The higher-frequency configuration failed to flutter at both M = 1.31 and M = 1.65 while the second lower-frequency configuration was tested at only M = 1.65 and fluttered successfully in the chordwise bending mode. During this test the blades were severely damaged and testing was terminated. Spectral analysis showed that the damaged cascade response contained two coexisting system modes (f = 245 Hz and f = 190 Hz), yielding a primary and secondary interblade phase angle. Since the blades were damaged during the first flutter event, the flutter boundary was only identified at M = 1.65.

TABLE OF CONTENTS

LIST OF ILLUSTRATIONS

LIST OF ILLUSTRATIONS (Cont'd)

LIST OF TABLES

INTRODUCTION

A. GENERAL

Contract N00019-74-C-0305 provides for an analytical and experimental investigation of features of supersonic chordwise bending flutter in airfoil cascades. This investigation is a significant part of an accelerating effort to develop improved design methods which will extend flutter-free compressor blade design into regions of high speeds appropriate to future generations of aircraft engines.

B. DEVELOPMENT TRENDS

Basic goals in fan and compressor design are to obtain increased pressure ratio per stage while maintaining acceptable efficiency and operating range. Tip speeds beyond 2000 ft/sec can be attained with concurrent pressure ratios beyond 2:1, and high efficiency. These high speeds and pressure ratios allow a reduction in the number of compressor and fan stages, and because higher tip speeds permit higher turbine velocity ratios, a reduction in the number of turbine stages and an increase in turbine efficiencies. The resulting engine is both shorter and lighter with a significantly greater thrust-to-weight ratio.

Still further improvements in engine weight can be achieved through the use of composite blading without part-span shrouds: in fact, for speeds above 2000 ft/sec, composites appear essential. The composite rotor can be considerably lighter than its titanium-bladed counterpart, and enable improved performance through the elimination of shrouds.

The design of advanced technology axial compressors has often involved a tradeoff between improved aerodynamic performance and structural integrity. As newer designs progress to higher pressure ratios and higher speeds, aeroelastic problems become more critical, especially those involving forms of flutter. Aeroelastic considerations are not new in the design of compressor blading. Many potential flutter problems have been successfully alleviated by structural design changes that incurred acceptably low performance penalties. Examples of such changes are increased blade thickness, added structural damping, and the use of part-span shrouds.

With the increased performance requirements of advanced designs, these solutions are becoming overly restrictive. For example, unacceptable penalties in performance will result from the use of conventional thickness blades in high speed rotors. Each of the mentioned aeromechanical improvements of increased tip speed and composite blades can move a fan or compressor rotor closer to a flutter boundary. Hence, it is important to understand the characteristics of the flutter phenomenon.

C. DESCRIPTION OF SUPERSONIC UNSTALLED FLUTTER

Figure 1 is a schematic compressor map with representative "boundaries" for four types of flutter. The map shows a typical compressor operating line, intersected by three constant speed lines, and bounded by the wide open discharge line at low pressure ratios, and the surge line at high pressure ratios. Flutter "boundaries" are contour lines of constant amplitude flutter stress, and as such are somewhat arbitrary, depending on the stress level selected to represent the boundary.

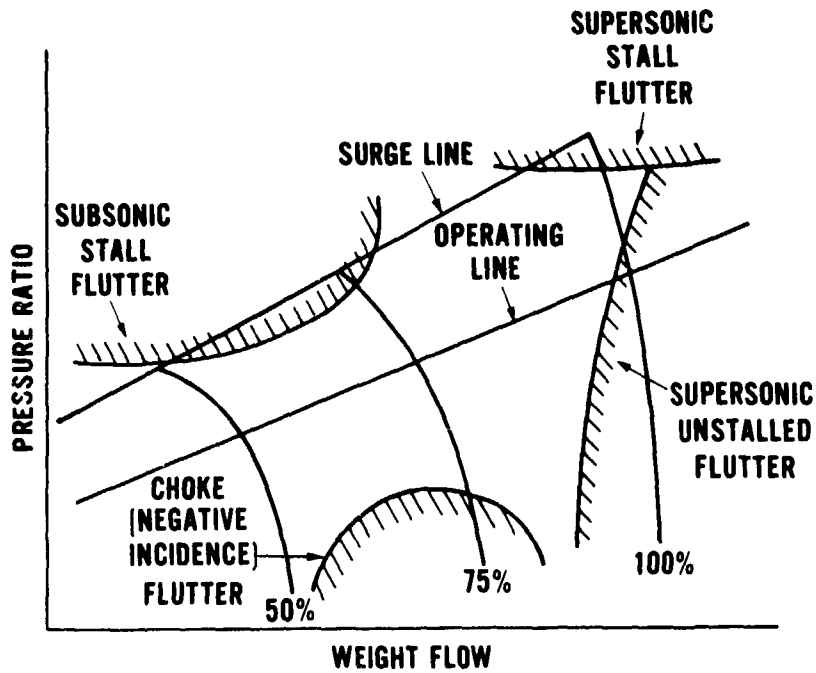

FIGURE 1 *Schematic Compressor Map Showing Flutter Boundaries for Four Types of Flutter*

Two types of flutter are of most concern: stall flutter and supersonic unstalled flutter. Stall flutter is characterized by self-excited blade vibration at operation near the surge line and may be identified by observing that the flutter stresses increase as the pressure ratio is raised. Supersonic unstalled flutter occurs when the outer span of the blade is operating supersonically; is somewhat stabilized by increasing back pressure; but can still occur at the design pressure ratio.

Supersonic unstalled flutter is of concern in either of two vibrational modes: one is the primarily torsional mode flutter investigated by P&WA under Contract N00019-72-C-0187; the other is the chordwise bending mode flutter subject to investigation in this program. References 1 through 5 discuss supersonic unstalled flutter in the torsional mode. The most important difference between this type of flutter and supersonic unstalled flutter in a chordwise bending mode may be described by referring to Figure 2. Figure 2 shows photographs of the

vibrational mode shapes of the first four modes of an 1800 ft/sec tip speed supersonic compressor blade. The photographs are of real time holograms of the vibrating airfoil. The fringe patterns indicate the relative vibrational amplitude of each mode, and the natural frequency of each mode is listed below the respective photograph Modes 1 and 3 are primarily bending modes; Mode 2 is primarily a torsional mode which was treated in Contract N00019-72-C-0187. Mode 4 is the lowest frequency chordwise bending mode for this blade. Mode 4 is different from modes 1, 2 and 3 because it involves a large vibrational deformation of the blade camber line while the other modes are primarily beam modes in which the chordwise deformation is small. Flutter in the chordwise bending mode is of great concern for the thin, high speed blades that are now being designed. The possibility of predicting flutter in chordwise bending mode was explored by using the theory of References 3 and 4 to calculate the aerodynamic damping for a typical chordwise blade deformation (Reference 6 and Appendix I) and it was found that the system might indeed become unstable with increasing Mach number.

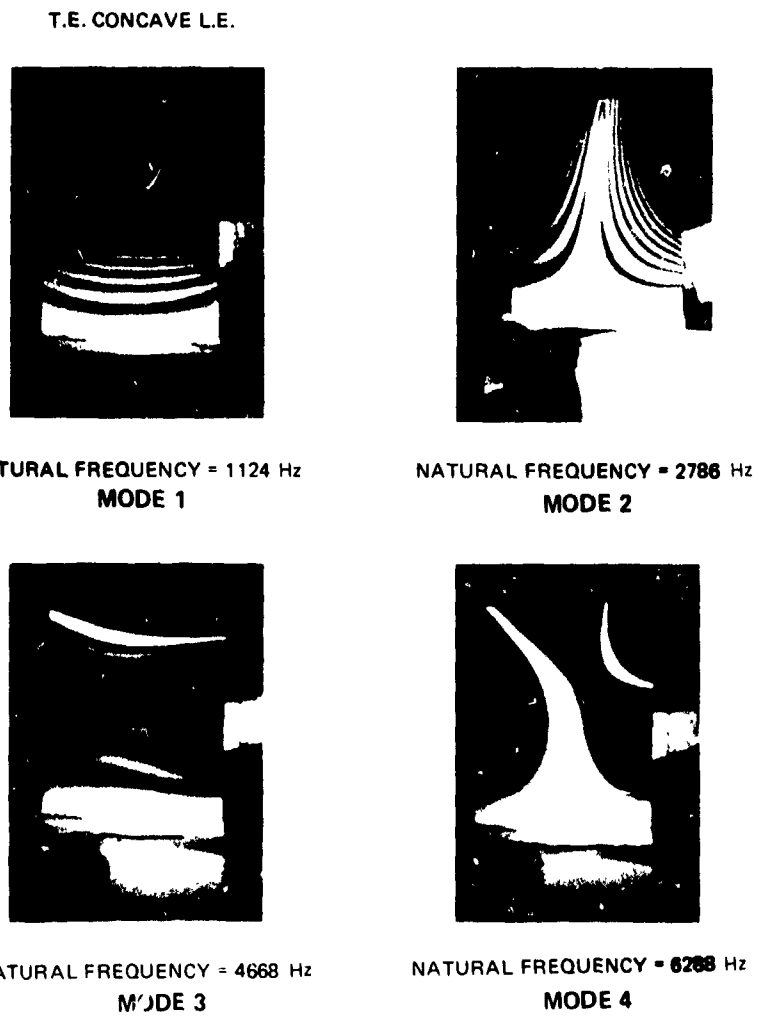

FIGURE 2 *Photographs of Holograms of First Four Vibrational Modes of P&WA 1800 ft/sec Compressor Research Rig Blade*

These results served as the impetus for the experimental chordwise supersonic bending flutter program performed at the United Technologies Research Center (UTRC) and reported in detail in Reference 7. Because this is the first time this type of flutter was systematically studied, the present program was exploratory in nature. In the course of this study, for example, it was essential to examine in detail the structural dynamic response of blade systems undergoing vibratory chordwise deformations, and to evaluate the various modes in terms of their susceptibility to aerodynamic excitation. The main objective at the outset of this program was to experimentally achieve the free-flutter of cascaded airfoils in a chordwise bending mode under controlled conditions. After this type of flutter was obtained, subsequent objectives included the identification of the flutter boundary over a range of supersonic Mach numbers and wind tunnel backpressures, as well as analyzing, via spectral techniques, the dynamic response data to evaluate the system behavior for each flutter incident.

RESEARCH FACILITIES

A. SUPERSONIC CASCADE WIND TUNNEL

A schematic diagram of the UTRC Supersonic Cascade Wind Tunnel is shown in Figure 3. Air supplied by laboratory compressors is expanded through interchangeable nozzle blocks to establish supersonic flow in the four-inch wide by approximately eight-inch high test section. The tunnel may be operated over a range of Mach numbers from 1.3 to 2.0. Downstream of the test section, suction is applied to provide the desired static pressure ratio across the cascade which consists typically of five blades plus upper and lower boundary layer scoops. Since the boundary layer scoops are contoured to the blade shape, the resulting cascade forms six blade passages.

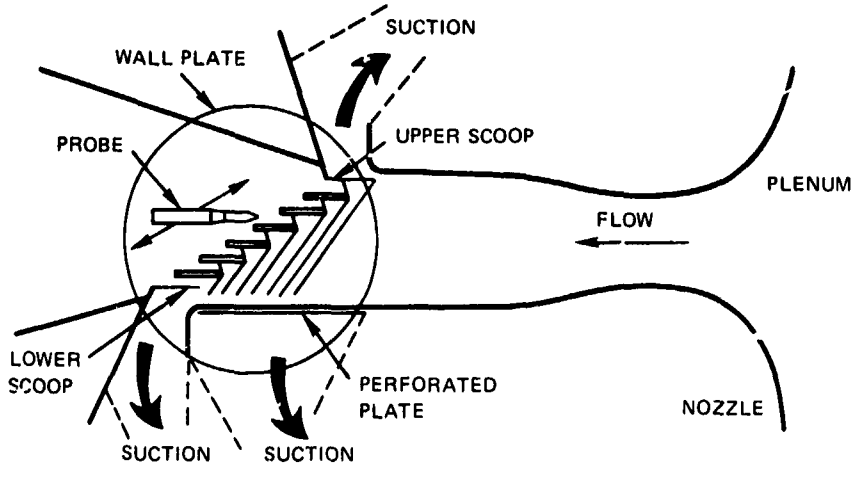

FIGURE 3 Supersonic Cascade Wind Tunnel

In this test the blades were cantilevered at both walls of the test section. One wall plate was made of steel and contained wedge-shaped openings that allowed the insertion of the matching wedge-shaped shanks of the blades. The other wall plate was made of Lucite, and contained narrow machined slots which were fitted to the mating tabs at the other span-end of the blades. The entire unit was assembled outside the tunnel as an integral system which permitted vibration bench testing of the entire blade pack. 'Detailed discussions of blade construction and system dynamics appear in subsequent sections.) During the flutter tests the unit was mounted in the wind tunnel such that the blade suction surfaces were parallel to the upstream flow. In a typical test run the pressure ratio across the test section can be changed independently of the upstream approach flow. This is accomplished by throttling the main flow passage downstream of the test section (i.e., raising the back pressure) while absorbing sufficient mass flow in the upper and lower boundary layer scoops to maintain the upstream mass flow at the same level as in the unthrottled condition. Ultimately, however,

if excessive throttling is applied the mass flow capacity of the boundary layer scoops is exceeded and flow is "spilled" from the cascade blade passages. At intermediate throttle settings the increased back pressure has been observed to cause normal shocks to exist within the blade passages while the leading edge regions remain unaffected. For the more conventional torsional flutter tests (Reference 1) it was found that increasing the back pressure was an effective method of controlling and even eliminating flutter. Another flow control system employed suction on the perforated floor plate just ahead of the test section (cf. Figure 3). In addition to removing part of the boundary layer, the perforated wall attenuated the leading edge shocks impinging on it, thus preventing them from reflecting back into the cascade.

Flow properties upstream of the cascade are measured through the use of wall static taps in the nozzle, and pitot and total temperature probes in the upstream plenum. The downstream flow properties can be measured with static taps in the side walls or with a traversing static pressure probe in combination with a pitot-static probe in the tunnel plane of symmetry. In view of the important contribution of the wakes to unsteady force and moment, the traversing probe was not used since it would disrupt the wakes. Furthermore, the only parameter of concern downstream of the cascade in these flutter tests was the static pressure used to determine the pressure ratio across the cascade. Using these measurements, the free stream Mach number, density, speed of sound, mass flow and pressure ratio are defined for each test point.

The coordinates of the J-blades tested herein are tabulated in Table 1. This blade is cambered, asymmetrical, and approximately 2.5 percent thick. The forward 50 percent of the chord is wedge-shaped with 0.008-inch radii at the leading and trailing edges.

TABLE I

TABULATED COORDINATES OF J-BLADE AIRFOILS

X	$Y_{suction}$	$Y_{pressure}$	X	$Y_{suction}$	$Y_{pressure}$
0.00000	0.00786	-0.00785	1.69510	0.06413	-0.01328
0.15410	0.01307	-0.00835	1.84920	0.06622	-0.01349
0.30820	0.01828	-0.00855	2.00330	0.06622	-0.01349
0.46230	0.02348	-0.00935	2.15740	0.06413	-0.01328
0.61640	0.02869	-0.00985	2.31150	0.05995	-0.01285
0.77050	0.03390	-0.01035	2.46560	0.05368	-0.01221
0.92460	0.03911	-0.01085	2.61970	0.04531	-0.01136
1.07870	0.04432	-0.01136	2.77380	0.03484	-0.01030
1.23250	0.04983	-0.01186	2.92790	0.02227	-0.00922
1.38690	0.05474	-0.01236	3.07364	0.00000	-0.00763
1.54100	0.05995	-0.01286	3.08200	0.00000	-0.00000

The shank end of each blade was wedge-shaped to fit into similarly shaped receptacles in the mirrored steel wall plate. Once inserted, these wedges were secured tightly in the wall plate slot by means of outside torque bolts. The other end of each blade, called the tab end, had a narrow tab which fitted tightly into a mating slot in the Lucite wall plate and was secured in place with a cyanoacrylate adhesive. Since the individual blades were intrinsically dissimilar in both mass distribution and in the degree of fixity of the tab end in the Lucite wall plate, the chordwise mode of interest for each of the blades had to be tuned to a common frequency prior to the installation of the blade pack in the wind tunnel for flutter testing. Furthermore, because both the frequency response and the logarithmic decrement are sensitive to the mounting at each end of the span, the tuning process was carried out outside the tunnel test area with the blades already mounted securely to the wall-plate and Lucite window. The entire system was then installed into the tunnel test section as a unit. The blades were numbered with blade 1 near the tunnel ceiling and blade 5 near the tunnel floor. The normal gap between blades was 1.125 inches and the horizontal stagger spacing was 1.949 inches.

B. INSTRUMENTATION

The three center blades of the cascade, numbered 2, 3, and 4, were each instrumented with two pairs of strain gages using a two-active leg circuit for each pair. Both pairs were located on the aft portion of the blades near the shank next to the wall-plate. Their specific locations were at points corresponding to high holographic fringe pattern curvature for maximum response. At these locations, the gages were oriented normal to the local fringe pattern corresponding to the direction of the stress vector. The measured response of the aft gage pair was out of phase with respect to the response of the forward gage pair. The outer two blades, numbered 1 and 5, were instrumented with one pair of gages each for monitoring purposes. Their location and orientation were the same as the forward gage pair on blades 2 and 3. Thus, a total of eight strain gage circuits were employed during this test.

The basic system used for recording the data, as discussed in Reference 7, is referred to as the WISARD (Wideband System for Acquiring and Recording Data).

High frequency noise was minimized by filtering the amplifier output above 10,000 Hz. Since this frequency is more than twice as high as the tenth harmonic of the highest natural frequency of the test, no signal attenuation in the frequency range of interest was possible. The amplified, filtered strain gage signals were recorded directly on FM tape using a CEC (model VR-3400) fourteen-channel variable speed tape recorder. In this system, the input data was recorded on the FM tape through two separate seven-channel magnetic recording heads. Similarly, playback for digitizing was accomplished through a pair of separate seven-channel magnetic playback heads. As standard procedure the recording and playback heads were carefully aligned to avoid inter-channel phase errors. However, to eliminate phase errors completely between as many of the eight strain gage data channels as possible, six of the gage outputs and the time code were recorded by one magnetic head. The two remaining gage outputs, corresponding to the rear gage of blade 2 and the single gage of blade 5, were recorded on the other magnetic head.

The data processing procedure required that analog signals from the FM tape be converted to digital form. This conversion is also done on the WISARD. Here, the operating flexibility of the data system permitted the frequency resolution of each unsteady signal to be maximized, regardless of the oscillation frequency. By recording the data at any of a number of selected tape speeds, and playing it back at a slower speed, it is possible to obtain test information at higher frequencies than would otherwise be possible if recording and playback speeds were equal. For the present data acquisition setup, the recording speed was set at 7½ inches per second and playback speed at 1-7/8 inches per second thus providing a time dilation factor of 4 for improved resolution of the waveform response.

PREDICTED PARAMETRIC EFFECTS ON FLUTTER SENSITIVITY

This section presents several results of applying the P&WA supersonic cascade aerodynamic damping analysis (Appendix I). The aeroelastic analysis was used to determine the effects of changing rotor speed (relative inlet velocity and Mach number) and changing reduced velocity holding Mach number constant for two different blade attachment geometries. The first of these studies was conducted to provide information on how the cascade flutter tests should be conducted. The reduced velocity study was conducted to determine the sensitivity of various mode shapes to changes in blade frequency.

Two different blade attachment geometries were analyzed: the single-cantilever attachment and the 43% double-cantilever attachment; and in addition, the first five modes of each blade attachment geometry were analyzed (see Appendix II). The modes of the single-cantilever attached blade are relatively uncoupled modes while the 43% double-cantilevered modes are highly coupled (see Appendix II). Unless otherwise stated, the nominal aerodynamic conditions given correspond to those in Table II.

Figures 4a and 4b show the effect on aerodynamic damping of changing Mach number and velocity concurrently (speed of sound = 1000 feet per second). In all cases, as Mach number and velocity increase the aerodynamic damping decreases. In the single-cantilever attachment, the torsion mode (mode 2) shows the greatest damping sensitivity to rotor speed, and the second torsion mode (mode 4) shows the least sensitivity. For the double-cantilever attachment, mode 1 shows the greatest damping sensitivity to rotor speed: mode 1 is a combination of bending, torsion and chordwise bending motions. Mode 5 shows the least sensitivity to rotor speed: mode 5 is primarily a chordwise bending mode. This study indicates that flutter should first be induced at the highest Mach number condition and then the blade should be further weakened to induce flutter at the lower Mach numbers.

Figures 5a and 5b show the effect of changes in reduced frequency on aerodynamic damping. For each mode, the frequency was varied ±10% about the nominal condition shown in Appendix II, Figure 13. For the single cantilever attachment all modes except the chordwise bending mode are stabilized by increases in reduced frequency. Between a reduced frequency of 0.92 and 1.02, the damping of the chordwise mode is predicted to experience a drop as frequency decreases. For the 43% double-cantilever mode all the modes are stabilized as reduced frequency is increased.

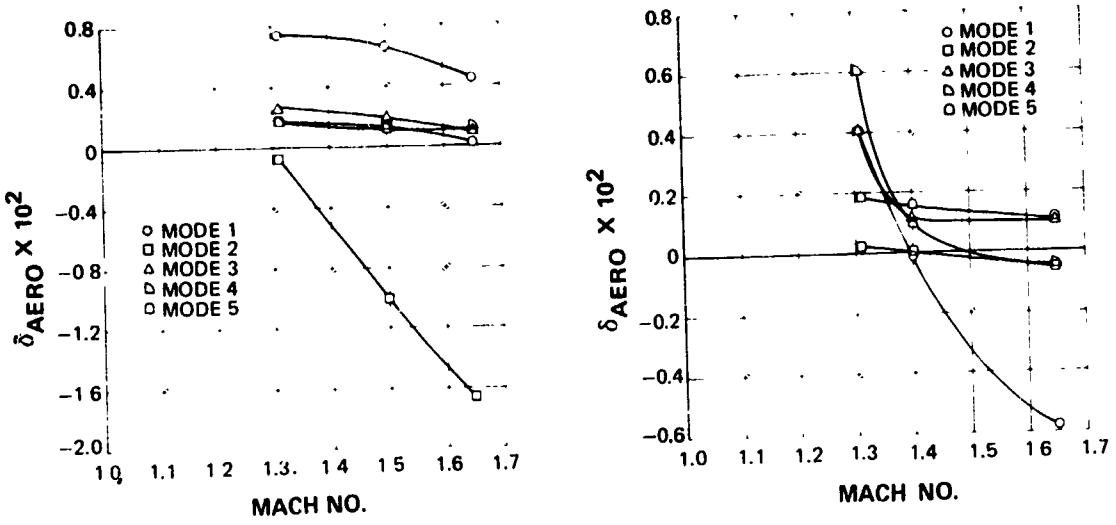

a) SINGLE-CANTILEVER ATTACHMENT

b) 43% DOUBLE-CANTILEVER ATTACHMENT

FIGURE 4 Effect of Rotor Speed on Aerodynamic Damping

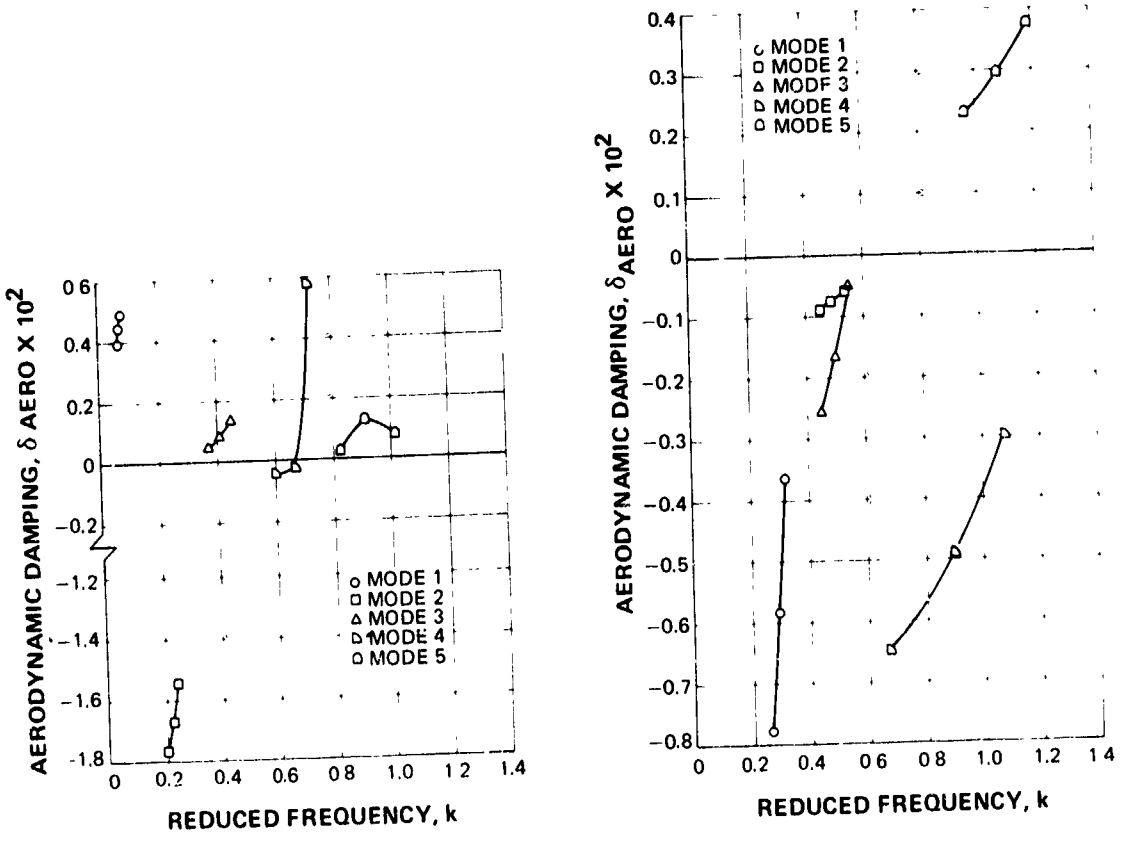

a) SINGLE-CANTILEVER ATTACHMENT

b) 43% DOUBLE-CANTILEVER ATTACHMENT

FIGURE 5 Effect of Reduced Frequency on Aerodynamic Damping

SELECTION OF TEST CONFIGURATION

Chordwise bending of the doubly-cantilevered blades in this program was originally envisioned as a primary deformation of the forward portion of the blade, more or less uniformly distributed over the entire span. Such a deformation would have its node-line(s) oriented mainly in the spanwise direction. It was expected that during flutter any two-dimensional chordwise section through the blade would have a behavior approaching that of an equivalent, variable thickness free-free beam, and that the resulting mode deformation would be greatest at the forward section with little or no motion aft of the midchord region. To ensure this type of behavior over the entire span, partial chordwise cuts were planned at each span end.

Bench tests were performed at UTRC in conjunction with NASTRAN computations and unsteady supersonic aerodynamic analyses, both of which were carried out at P&WA to serve as a guide in the selection of the modes most susceptible to chordwise bending flutter. Details of the P&WA analysis appear in Appendix II. The analysis shows that for the conventional single- or fully double-cantilevered blade support configuration, supersonic flutter was likely to occur only in the first torsion mode in which no chordwise deformation takes place. As chordwise cuts were introduced at both span ends, however, both low and high frequency modes exhibited some chordwise bending deformation. NASTRAN predictions indicated that the fourth mode in the frequency hierarchy of the 43 percent doubly-cantilevered blade would satisfy the objectives of this program and, accordingly, it became the initial mode of primary interest. However, during these calculations (cf. Appendix II), it was found that the first bending mode for this configuration might also be susceptible to flutter, but with a comparable amount of chordwise bending. Ultimately, this first mode became the flutter mode of primary interest after suitable modifications in the blade structure were made.

The initial bench tests were performed on a prototype J-blade configuration which approximated most of the important features of the actual test blades. This prototype was supported in steel clamps at both span ends and subjected to a variety of vibration tests while undergoing a sequence of blade attachment modifications consisting of various chordwise cuts (cf. Appendix III for details). This was done as part of the process of selecting the final test blade configuration for the supersonic flutter test. The results of these tests were in general agreement with the predictions of the NASTRAN program and also showed, as the cantilever support was reduced, that blade nonuniformities caused the modes to become increasingly asymmetric, especially the modes containing chordwise node lines. It was later determined that such effects could be corrected by fine tuning the final mode of interest.

Following the prototype tests, the actual blade hardware was vibration tested to determine which of several techniques was most appropriate for securing the tab end of the blade into the transparent Lucite window. Initial tests were carried out with the tab ends fixed in steel clamps. This end fixity was chosen to serve as a reference condition which was directly comparable to both the ideal double-cantilever attachment implicitly assumed in the NASTRAN model, and the all-steel prototype configuration just described. Two Lucite support

configurations were then tested as described in Appendix III. The final blade support arrangement chosen involved the insertion of accurately machined blade tabs into the tightly fitting matching slots of the Lucite window. A cyanoacrylate adhesive was used as a bonding agent. It is shown in Appendix III that this procedure yielded an end fixity comparable to the ideal steel clamp configuration.

As stated earlier, the fourth mode of the 43 percent doubly-cantilevered blade was the initial choice as the chordwise bending mode of primary interest. However, it was found, while bench testing the actual blades, that the frequencies of modes 4 and 5 were very close to one another. Interference between these two neighboring modes would be intolerable during aerodynamic testing. Because of this, and the desirability of lowering the frequency of mode 4 to increase the possibility of chordwise bending flutter, it was decided to introduce a spanwise groove on the suction side of the blade midchord region (shown in Figure 6). The spanwise groove would serve three purposes: it would (a) separate modes 4 and 5, (b) lower the frequency of mode 4, and (c) increase the amount of mode 4 chordwise bending curvature. In subsequent NASTRAN analyses of the grooved configuration it was found, for the 43 percent double-cantilever support, that mode 1 (originally a pure fully-doubly-cantilevered first bending mode) exhibited as much chordwise deformation as mode 4, and at a much lower frequency. Furthermore, aerodynamic calculations indicated that mode 1 would flutter more readily than mode 4. On this basis, mode 1 was chosen as the primary mode of interest for all subsequent work. Results of these analyses and other details of the grooved configuration are found in Appendix IV.

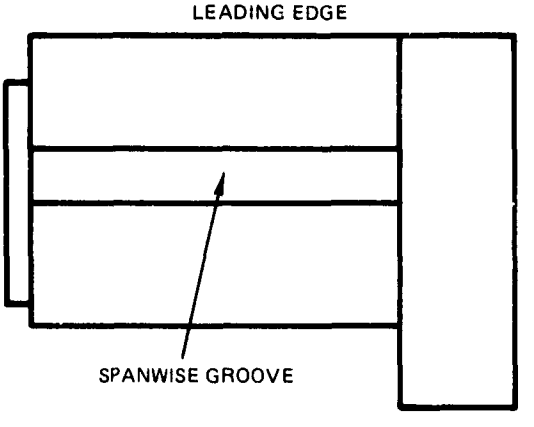

FIGURE 6 Plan View of Blade Showing Spanwise Groove

Two materials were used at separate times to fill the spanwise groove in order to retain the original aerodynamic shape of the blades. The first filler was a dense epoxy having approximately 70 percent of the blade material density. The object in using this substance was to effectively reduce the chordwise stiffness. However, after curing, it was found that the epoxy actually raised the stiffness of the grooved blade and also raised its mechanical damping. When this configuration was tested aerodynamically (see next section) flutter did not occur; however, low-amplitude, sporadic buffeting was observed. In addition, small pieces of this material broke away during the test and, consequently, altered the aerodynamic shape of the blades.

The second filler used was an RTV silicone rubber sealer which was ideal in most respects. In addition to filling the cavity, it had little or no effect on blade damping and contributed nothing to the stiffness. No deterioration of this material occurred during subsequent bench tests and the aerodynamic flutter test.

In order to ensure flutter for this configuration, additional 0.4-inch cuts were made in the spanwise direction (shown schematically at A and B on Figure 7). This caused a further reduction in the frequency of mode 1. The details of this process are presented in Appendix V.

Prior to flutter testing each of the two configurations described above, each blade had been individually rough-tuned to a target frequency and then mounted in cascade into the mirrored wall-plate and Lucite window. The entire system was then secured to a portable rigid frame which simulated the support provided by the wind tunnel walls. The entire assembled system was then bench tested and fine-tuned to a common interblade mode 1 frequency. The details of this procedure are also given in Appendix V.

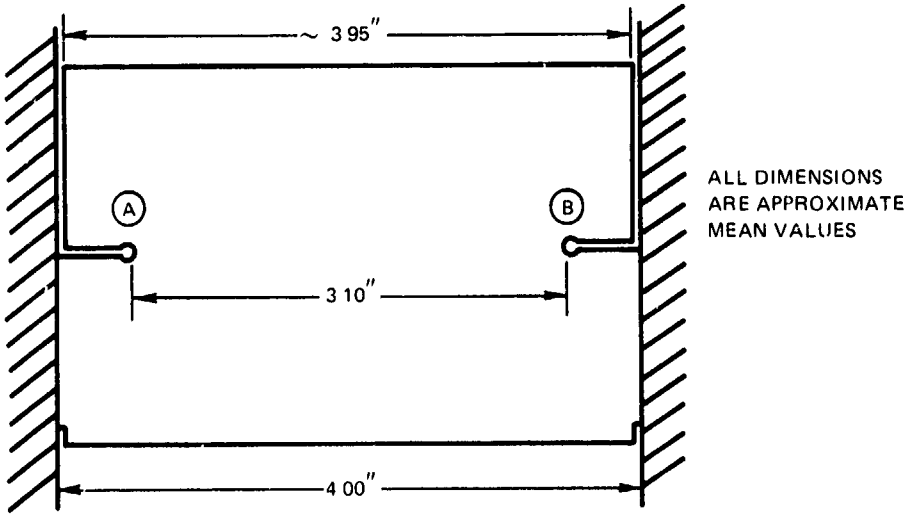

FIGURE 7 Plan View of Blade Showing Chordwise and Spanwise Cuts

FLUTTER TEST

A. WIND TUNNEL TEST PROCEDURE

Supersonic aerodynamic tests were performed on the tuned blade system by following the procedures outlined in an earlier section. In the first test program each of the blades contained a spanwise groove in the midchord region which was filled with a dense epoxy (cf. Figure 6 and Appendix IV). These grooves, in combination with chordwise cuts over 63 percent of the chord at each span end (Figure 24 in Appendix IV) of the tuned system, provided a uniform interblade frequency of 423 Hz. Tests were conducted at both M = 1.31 and M = 1.65. In each case the test section temperature was raised to 180°F to eliminate flow condensation. Higher temperatures were avoided to prevent the deterioration of both the epoxy filler and strain gage adhesive. During this test program the pressure ratio across the test section was varied from the wide open condition (approximately 1.25) to the spill condition with no occurrence of chordwise flutter. At the higher pressure ratios some low-amplitude sporadic buffeting took place, but in general the system was considered to be stable.

A modified cascade system, which was more susceptible to chordwise bending flutter, was tested next at M = 1.65. This configuration consisted of blades that contained RTV filler in the spanwise grooves and a combination of chordwise cuts over 63 percent of the chord at each span end and 0.4 inch spanwise cuts at each span end near the midchord region (cf. Figure 7 and Appendix IV). This configuration was tuned to a uniform interblade frequency of 360 Hz in the chordwise bending mode (mode 1).

Violent chordwise bending flutter occurred as soon as M = 1.65 was attained, and all efforts to diminish or control the flutter by varying back pressure were ineffective. It was determined visually that blade 3 was oscillating with an amplitude of approximately 0.1 inch at the midspan leading edge, and the other blades were oscillating at somewhat smaller (but still significant) amplitudes of approximately 0.05 inch or greater. No attempt was made to raise the airflow temperature because it was felt that the blades would fail long before the desired temperature could be reached. Therefore, this test was conducted at a test section temperature of T = 55°F. Even at this low temperature, however, no condensation was visible in the test section during this run. A long data record was taken (approximately 1 minute of real-time data) and the test was terminated.

B. POST EXPERIMENT BLADE EXAMINATION

Following the test, a visual examination of the individual blades was made and it was found that significant fatigue damage had occurred on blades 1, 2, and 3. Specifically, with reference to Figure 7:

i) blade 1 sustained a thin crack starting at A and extending approximately ¾ inches in the span direction,

ii) blade 2 sustained a hairline fracture starting at B and extending about ¼ inch in the span direction,

iii) blade 3 suffered a severe fracture which started at B and extended about 1¼ inches in the span direction, and

iv) blades 4 and 5 sustained no visible damage, although it is possible that some internal damage may have occurred.

The results from an analysis of the dynamic response signals on the FM tape (see below) showed that flutter had occurred at a primary frequency of approximately 245 Hz with some secondary response occurring at 190 Hz. From this test, it can be concluded that although incipient chordwise bending flutter occurred readily at M = 1.65 for a cascade tuned to a uniform interblade frequency of 360 Hz, progressive blade fatigue damage caused the cascade frequency response to drop as flutter continued to occur.

Bench vibration tests were then performed on the damaged blade pack. Initial tests on all blades at very low amplitudes yielded frequencies that were considerably higher than the observed flutter frequencies, and in some cases were nearly equal to the frequencies of the undamaged blades. Additional vibration tests on the damaged blades at higher excitation amplitudes showed that their frequencies dropped as the amplitude was increased (details appear in Appendix VI). Thus, it was surmised that the spanwise cracks caused a nonlinear softening of the blade stiffness in that the effective stiffness of the cracked blade was a decreasing function of amplitude. This is discussed in Appendix VI, together with a brief analysis which lends credence to the soft-spring hypothesis.

C. RESULTS OF FLUTTER TEST

Because blade fatigue failure occurred in the test just described, the chordwise bending flutter program was terminated and only one flutter condition was documented. Consequently, it is impossible to define a stability boundary for chordwise bending flutter. However, based on this single flutter condition and the two stable conditions obtained from the previous test, some conjectures on such a flutter boundary can be made by utilizing the trend lines predicted from a supersonic analysis based on supersonic cascade theory (Appendix I).

The parameters of interest here are the Mach number, M, the reduced frequency based on chord, $\omega = 2\pi fc/V$, and the compressible reduced frequency

$$k = \frac{\omega M}{M^2-1} = \frac{2\pi fc}{a(M^2-1)},$$

where a is the local speed of sound and c is the blade chord. Table II contains the values of these parameters for three test conditions of this study.

TABLE II

TEST CONDITIONS

RESULT	M	T(°R)	V(ft/sec)	f (Hz)	ω	k
No flutter	1.31	640	1625	423	0.421	0.770
No flutter	1.65	640	2047	423	0.334	0.320
Flutter	1.65	515	1836	360	0.317	0.307
	1.65	515	1836	245	0.216	0.209

The first three listed frequencies were those obtained in the bench test prior to testing. In the third case, flutter initiated at f = 360 Hz and continued as the frequency dropped to the final value of approximately 245 Hz. These test points are shown in the upper two panels of Figure 8 for Mach number versus both compressible reduced frequency, k, in Figure 8a, and versus reduced frequency, ω, in Figure 8b. (Open symbols denote no flutter and solid symbols denote flutter.) The line connecting the two solid symbols shows the extent of the frequency change from flutter initiation at 360 Hz to test termination at 245 Hz.

Supplementary calculations of aerodynamic damping for this flutter mode were carried out and are shown in Figure 8c for three Mach numbers, M = 1.4, 1.65, and 1.8. The value $\delta = 0$ represents the customary incipient flutter boundary for undamped systems, and is plotted in Figures 8a and 8b. It is seen that this result does not agree well with measured data. However, it was noted that the average mechanical damping of the test cascade prior to testing was approximately $\delta = 0.015$. Therefore, a compensating negative aerodynamic damping level of -0.015 was also plotted which is in better agreement with measured data. Finally, the curve for $\delta = -0.030$ was plotted, and it is seen that this value is in good agreement with the initial measured flutter point at 360 Hz.

These results may be interpreted as follows. Although the no-flow system damping for each blade was approximately $\delta = 0.015$, there may be additional system damping which caused the total damping to be as high as $\delta = 0.030$ during the flutter test. This may be associated with the large damping of blade 5 (noted in Appendix V), or more probably, may be an effect of the finite number of blades in the test cascade. If either of these conjectures is true, and if the constant damping line, corresponding to $\delta = 0.030$, is the flutter boundary, then an extrapolation of this curve in Figures 8a or 8b to M = 1.3 shows the test condition at the lower Mach number to be more stable than the same configuration tested at M = 1.65. Furthermore, this indicates that the test condition at M = 1.65 and f = 423 Hz was only marginally stable.

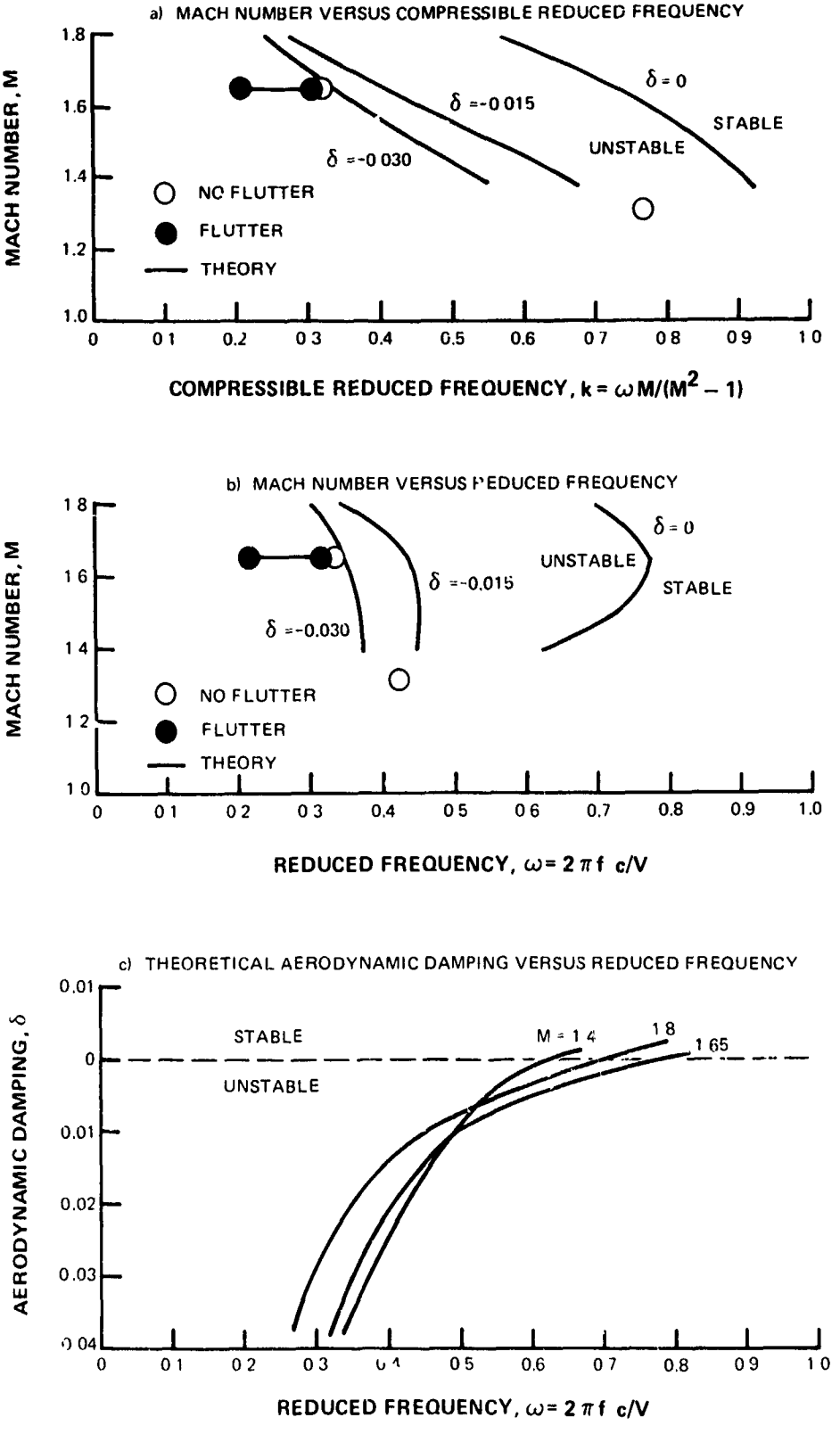

FIGURE 8 *Comparison of Theoretical and Experimental Flutter Stability*

D. SPECTRAL ANALYSIS

It was stated earlier that during flutter a long real-time record was taken of the flutter response on FM tape. A subsequent visual examination of the record showed some irregularities in the amplitudes and frequencies of the various blades. Specifically, the dynamic stress response of blade 2 appeared to be the most consistent in that its basic frequency was always approximately 245 ±5 Hz, and its amplitude was almost always higher than the other blades in the pack. Conversely, the stress response of blade 3 appeared to be the most irregular in that its frequency shifted alternately between 245 Hz and 190 Hz. Hence, several regions of this flutter record were chosen for analysis to illustrate a variety of interblade dynamic activity, including situations in which the dominant frequency was 245 Hz on all blades, and those in which a mixture of frequencies was evident. Some representative examples of these selected points are shown in the upper plots of Figures 9 through 13. In each case the time history of blades 1 through 4 are shown. (The single strain gage pair on blade 5 failed during the test and no record of its motion was obtained.) No scale is placed on the ordinate since the recorded stress amplitude is probably not meaningful for cracked blades. However, the relative harmonic amplitudes for each blade response are important and are used in the discussion of the results below.

Other characteristics of the signal which are useful were obtained by performing a spectral analysis of these points. A discussion of the application of spectral analysis to these data is found in Appendix VII. The results of the spectral analysis useful to this program are the amplitude response at the peak frequencies, obtained from the autocorrelation of the signal, and the corresponding interblade phase angle at these frequency peaks, obtained from the crosscorrelation of the signal. Results of such an analysis are plotted versus blade number in the lower three panels of each of Figures 9 through 13. The lower left panel shows the interblade phase lead angle of each blade relative to blade 1 for the response at 245 Hz, and in the center figure is the interblade phase angle for the response at 190 Hz. The bar graph at the lower right shows the amplitude ratio of the peak response at 245 Hz to the peak response at 190 Hz, A_{245}/A_{190}, for each blade. This is a measure of the relative amplitude content of each frequency component for each blade. To clarify these concepts, consider these figures in detail.

The selected points are chronologically arranged in Figures 9 through 13 and are denoted, for convenience, as points 1 through 5. Point 1 in Figure 9 has a dominant 245 Hz response, as seen in the time history and in the harmonic amplitude ratios for all blades. This was the only condition analyzed in which no meaningful interblade phase angle data could be obtained at f = 190 Hz. In the lower left panel, the straight line correlation between the interblade phase lead angles for blades 2 and 4 relative to blade 1 indicates the presence of a system flutter mode at a relative interblade phase angle per blade of approximately 75 deg (which would represent a forward travelling wave in a rotating blade row). Note, however, that blade 3 did not participate in the system mode but instead is nearly in phase with its upper adjacent neighbor, blade 2. This behavior is repeated in subsequent figures. A closer examination of the harmonic amplitude ratio in Figure 9 shows that all blades were predominantly oscillating in the higher frequency mode. Even blade 3, which tended in most other cases to have a large harmonic content at the lower frequency, had a harmonic amplitude ratio of 3.

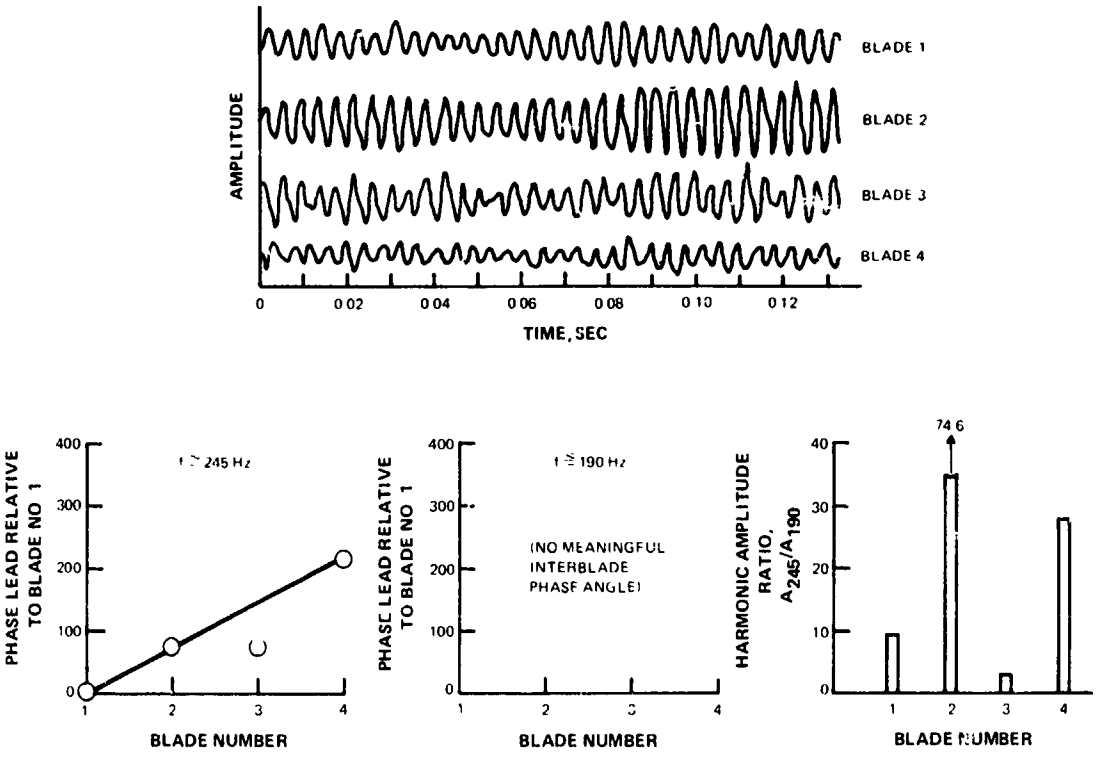

FIGURE 9 Flutter Waveform and Statistically Averaged Results: Point 1

In Figure 10 for point 2 the time history shows blade 2 was still oscillating at 245 Hz, but blade 3 was now oscillating primarily at 190 Hz. Neither of these were dominant modes as evidenced by both the lower value of the harmonic amplitude ratio for all blades (nearly equal to 1.0 for blades 1, 3, and 4) and the ability of the spectral analysis procedure to calculate an interblade phase angle for both frequencies. Once again the system mode for 245 Hz had a relative interblade phase angle per blade of approximately 75 deg, and once again blade 3 was nearly in phase with blade 2. At the lower frequency the relative interblade phase angle per blade was approximately 125 deg (center figure) and blade 2 was not correlated. This is not surprising because blade 2 had very little 190 Hz content as shown in the bar graph. Figures 11, 12, and 13 for points 3, 4, and 5 continue to show this same trend with minor variations in the values of the parameters. The value of interblade phase angle for blade 2 is missing in Figure 11 because blade 2 was uncorrelated with the other blades at 190 Hz. Correspondingly, the time history in this instance shows a very dominant 245 Hz response for blade 2.

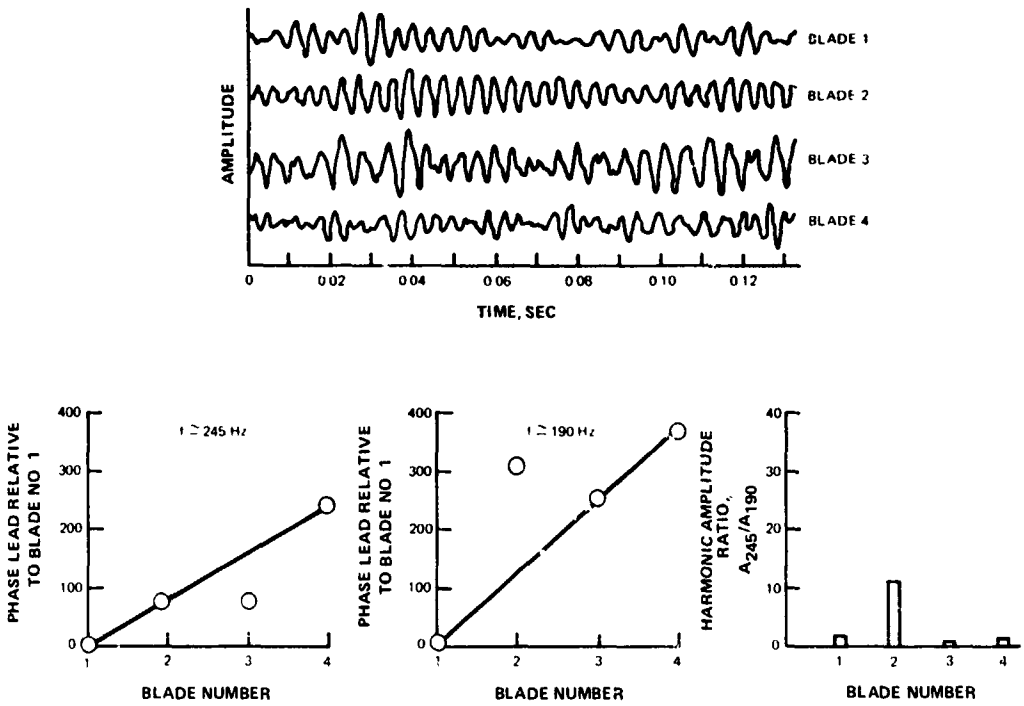

FIGURE 10 Flutter Waveform and Statistically Averaged Results: Point 2

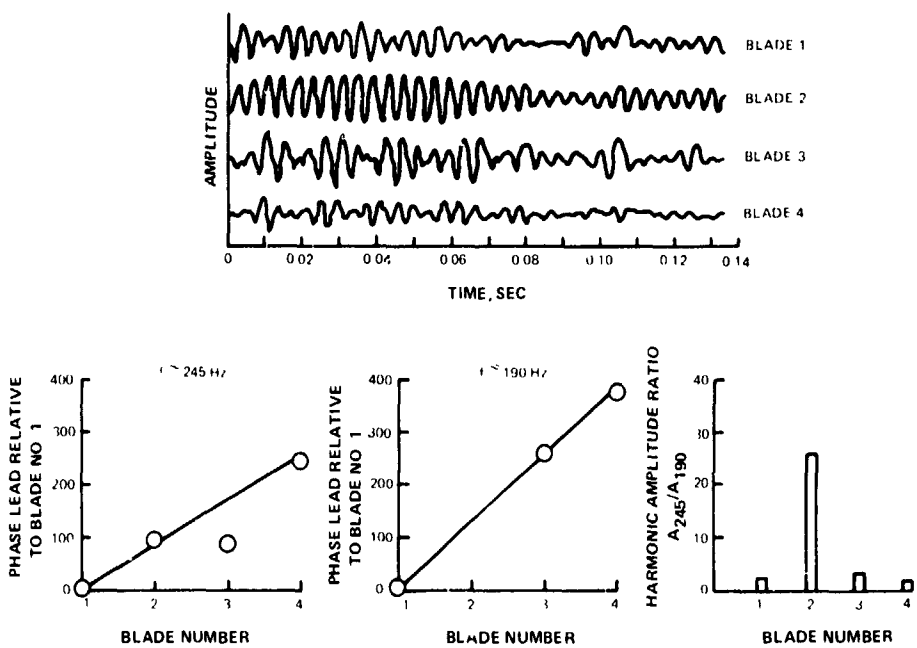

FIGURE 11 Flutter Waveform and Statistically Averaged Results: Point 3

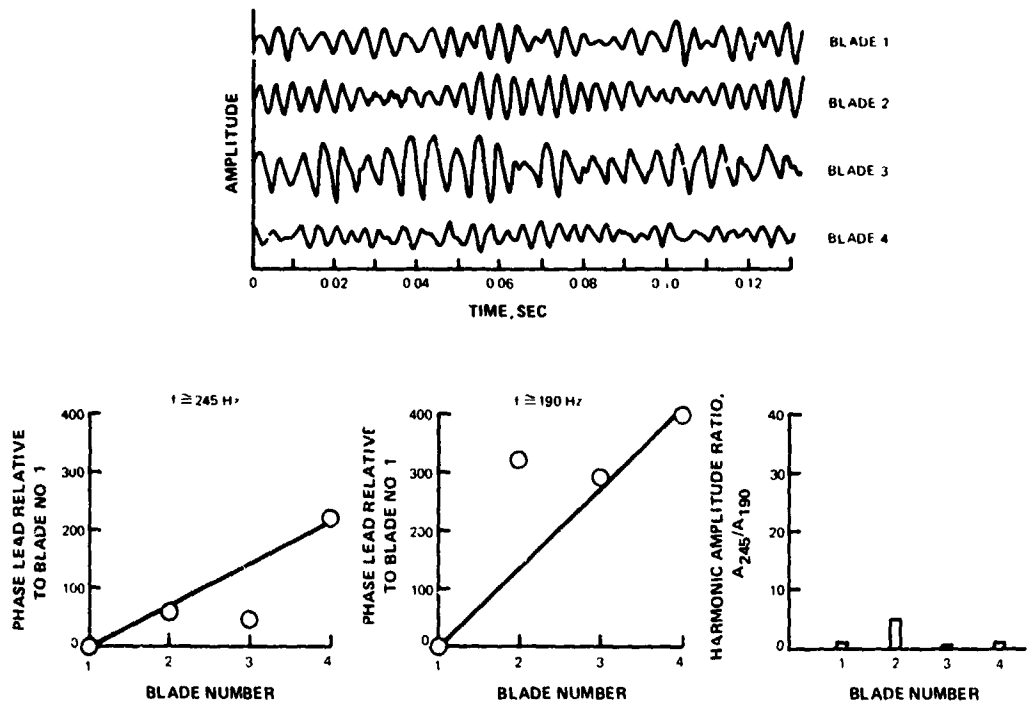

FIGURE 12 Flutter Waveform and Statistically Averaged Results: Point 4

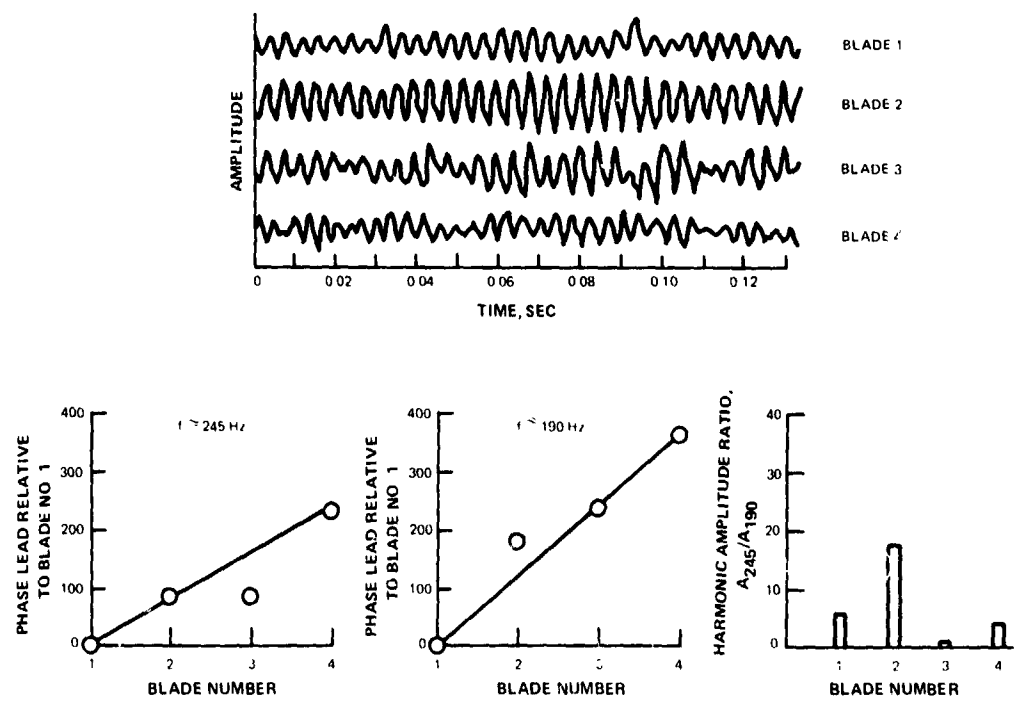

FIGURE 13 Flutter Waveform and Statistically Averaged Results: Point 5

CONCLUSIONS

The foregoing results and accompanying discussion represent a first attempt at systematically investigating the phenomenon of chordwise bending flutter. Although chordwise bending flutter was successfully demonstrated in the UTRC supersonic cascade tunnel facility, only one flutter case was recorded and subsequently analyzed since the cascade blading sustained severe fatigue damage during the first flutter event. Therefore, only a few conclusions (some of which may be tentative) could be drawn from the analysis.

1. Cascade flutter was demonstrated in a chordwise bending mode in supersonic flow (M = 1.65).

2. The flutter mode was the first bending mode of a fully double-cantilevered J-blade in which chordwise bending was enhanced by both removing 63% of the chordwise double-cantilever support at both span ends and removing half the blade thickness in the midchord region.

3. Although no flutter boundary was defined experimentally, the flutter point for M = 1.65 was determined within a narrow range of compressible reduced frequency ($0.307 \leqslant k \leqslant 0.320$). Specifically, at M = 1.65, flutter did not occur at f = 423 Hz and T = 180°F, but did occur at f = 360 Hz and T = 55°F.

4. Incipient flutter occurred at a uniform blade frequency of 360 Hz and continued to occur at a lower frequency even though some of the blades sustained enough damage to completely detune the cascade.

5. The damaged cascade was observed to vibrate at a uniform primary frequency approximately equal to the high-amplitude resonant value of the center blade (the most severely damaged blade) of the cascade.

6. A secondary system mode frequency (lower than the primary system mode frequency) was also observed. The source of this has also been tentatively attributed to the center blade dynamic response.

7. The interblade phase angle for the primary system mode (f = 245 Hz) was determined to be 75° (forward travelling wave) where the center blade was uncorrelated. The interblade phase angle for the secondary system mode (f = 190 Hz) was found to be 125° (forward travelling wave) where the blade immediately upstream of the center blade was uncorrelated.

REFERENCES

1. Snyder, L. E. and G. L. Commerford: Supersonic Unstalled Flutter in Fan Rotors; Analytical and Experimental Results. Transactions of the ASME, Journal of Engineering for Power, Ser. A, Vol. 96, No. 4, October 1974, pp. 379-386.

2. Snyder, L. E.: Supersonic Torsional Flutter in Cascades. Pratt and Whitney Aircraft Report No. PWA-4701, Final Technical Report, Contract N00019-72-C-0187, Naval Air Systems Command, 2 April 1973.

3. Verdon, J. M.: The Unsteady Aerodynamics of a Finite Supersonic Cascade with Subsonic Axial Flow. Transactions of the ASME, Journal of Applied Mechanics, Ser. E, Vol. 40, No. 3, September 1973, pp. 667-671.

4. Verdon, J. M. and J. E. McCune: Unsteady Supersonic Cascade in Subsonic Axial Flow. AIAA Journal, Vol. 13, No. 2, February 1975, pp. 193-201.

5. Mikolajczak, A. A., R. A. Arnoldi, L. E. Snyder, and H. Stargardter: Advances in Fan and Compressor Blade Flutter Analysis and Predictions. Presented at the AFOSR Symposium on Propulsion System Structural Integrity, Naval Post Graduate School, Monterey, California, September 1974. (To be published in the AIAA Journal of Aircraft, May 1975.)

6. Snyder, L. E.: Supersonic Chordwise Bending Flutter in Cascades. Report No. PWA-5061, First Quarterly Progress Report, Contract N00019-74-C-0305, Naval Air Systems Command, 1 August 1974.

7. St. Hilaire, A. O. and F. O. Carta: Supersonic Chordwise Bending Flutter of Cascaded Airfoils. UTRC Report No. R75-213304-1, 1975.

8. Ward, D. and W. Cohen: Wide Band System for Acquiring and Recording Data (WISARD). United Aircraft Research Laboratories Report H076944-1, October 1969.

9. Stetson, K. A.: Holographic Vibration Analysis. Chapter 7 of Holographic Nondestructive Testing, Academic Press, New York, 1974.

10. Stoker, J. J.: Nonlinear Vibrations. Interscience Publishers, New York, 1950.

APPENDIX I

UNSTEADY SUPERSONIC AERODYNAMICS FOR CHORDWISE BENDING VIBRATION

UNSTEADY AERODYNAMIC RESPONSE OF A CASCADE UNDERGOING A CHORDWISE BENDING VIBRATION IN SUPERSONIC FLOW

A method of calculating the unsteady aerodynamic response of cascade experiencing rigid beam vibration is presented in Reference 3. To modify this procedure to account for a vibration involving a significant deformation of the blade camber line requires only the reformulation of the surface upwash condition. The surface boundary condition for any unsteady airfoil motion is:

$$v'_n = \frac{Dy_n}{Dt} = \frac{\partial y_n}{\partial t} + U\frac{\partial y_n}{\partial x} \tag{1}$$

where subscript refers to the n^{th} blade in the cascade.

For the harmonic oscillation of a cascade of plates, the vibratory deflection normal to the blade camber line takes the form:

$$y_n\ (x, t) = y_n(x)e^{i(\omega t + \sigma_n)} \tag{2}$$

where σ_n is the interblade phase angle.

The function $y_n\ (x)$ can be expressed as a polynomial function of x with variable coefficients of the form

$$y_n = A_1 x^2 + A_2 x + A_3$$

or $$y_n\ (x, t) = [A_1 x^2 + A_2 x + A_3]\ e^{i(\omega t + \sigma_n)}$$

When this expression is placed into Equation (2), the final form of the upwash equation becomes

$$v'_n = [i\omega(A_1 x^2 + A_2 x + A_3) + U(2A_1 x + A_2)]e^{i(\omega t + \sigma_n)} \tag{3}$$

The normal velocity of the fluid on the blade surface is related to the velocity potential by

$$v'_n = \frac{\partial \phi_s}{\partial y} \tag{4}$$

Following the treatment of Reference (3), a modified velocity potential may be written:

$$\psi(x, y) = \phi(x, y, t)e^{i(kMx - \omega t)} \tag{5}$$

or $$\frac{\partial \psi}{\partial y} = \frac{\partial \phi}{\partial y} e^{i(kMx - \omega t)} = V'_n e^{i(kMx - \omega t)}$$

Using the upwash condition previously devised, the final form of the modified velocity potential for a chordwise bending vibration becomes:

$$\frac{\partial \psi}{\partial y} = [i\omega(A_1 x^2 + A_2 x + A_3) + U(2A_1 x + A_2)]e^{i(kMx + \sigma_n)} \tag{6}$$

Using this equation to replace Equation (4) in Reference 3, the unsteady pressure distribution, $\Delta p(x, t)$, for a chordwise bending vibration can be evaluated.

From the above pressure distribution, an expression for aerodynamic damping logarithmic decrement) can be obtained. This logarithmic decrement for a small amplitude motion is:

$$\delta_{aero} = \frac{W_{aero}}{4\overline{KE}} \tag{7}$$

where: W_{aero} = aerodynamic work/cycle due to fluctuating pressure

$\overline{KE}$ = average system kinetic energy.

The aerodynamic work/cycle done by the air on the blade is:

$$W_{aero} = \int_{r_o}^{r_t} \int_{o}^{2\pi} \int_{o}^{2b} \Delta p(x, t) \cdot y_n(x, t)\, dx\, d\omega t\, dr \tag{8}$$

where r_o and r_t are the root and tip radius respectively and b is the blade semichord.

From the above system of equations, the system stability can be calculated for a chordwise bending vibration given the vibratory mode shape.

APPENDIX II

PRELIMINARY NASTRAN ANALYSIS

As a preliminary step to the blade dynamics bench tests, the NASTRAN (NASA Structural Analysis) program, available at P&WA, was used to calculate the natural frequencies and mode shapes of the first five vibration modes of the J-blade profile. The purpose of this analysis was to determine which mode and what blade mounting configuration would most likely yield chordwise bending flutter. The first five natural modes of four blade attachment geometries were calculated: (a) cantilevered from one end; (b) fully cantilevered from both ends; (c) cantilevered from both ends over the aft 71% of the chord; and (d) cantilevered from both ends over the aft 43% of the chord. The airfoil coordinates are given in Table 1. The chord length and span width of the test blades are 3.09 inches and 4.00 inches, respectively, and the airfoil maximum thickness is 2.5% chord. The airfoil was modeled by the NASTRAN program with a grid having 15 chordwise and 21 spanwise elements. The results of these calculations are shown in Figure 14. In the first portion of this figure the modes shown can be generally classified as first bending, first torsion, second bending, second torsion, and first chordwise bending. All modes show some degree of chordwise deformation with modes four and five showing the greater amount. The details of the modes show that a three-dimensional finite element analysis will differ considerably from the results of a beam analysis for this blade geometry. As the aspect ratio of the blade is lowered, this difference would be expected to become even more pronounced.

The first five modes for the double-cantilever airfoil are shown in Figure 14b. The effect of attaching each end of the airfoil in a cantilevered manner is to raise the mode frequencies and to increase the amount of chordwise deformation present in each mode. The modes for this attachment can be classified as first bending, first torsion, second bending, first chordwise bending and second torsion. The third attachment geometry corresponds to cutting the airfoil attachment at each span end back 29% from the leading edge. The resulting mode shapes are shown in Figure 14c. The first three modes are again first bending, first torsion and second bending type modes; however, modes four and five are related chordwise bending modes. The fourth attachment geometry corresponds to cutting the airfoil attachment at each span end 57% from the leading edge. The resulting mode shapes, as shown in Figure 14d, are difficult to relate to simple two-dimensional modes. These modes are highly three-dimensional with a large amount of chordwise bending deformation.

The aerodynamic damping, logarithmic decrement (δ) for each of the modes displayed in Figure 14a-d, was calculated by the unstalled supersonic flutter analysis of Appendix I.

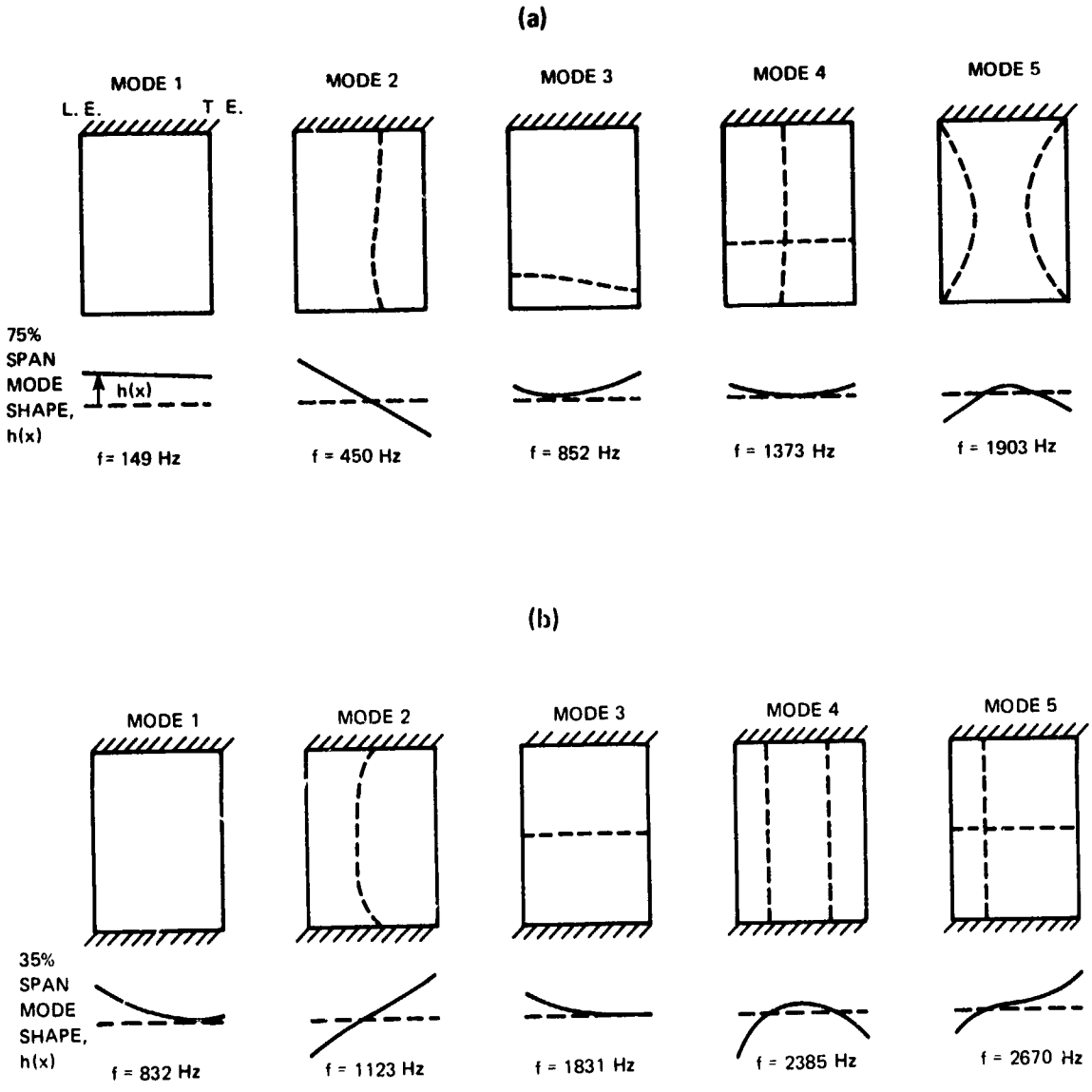

FIGURE 14 *NASTRAN Results – J-Blade Profile*
(a) Single-Cantilever Attachment
(b) Double-Cantilever Attachment

(c)

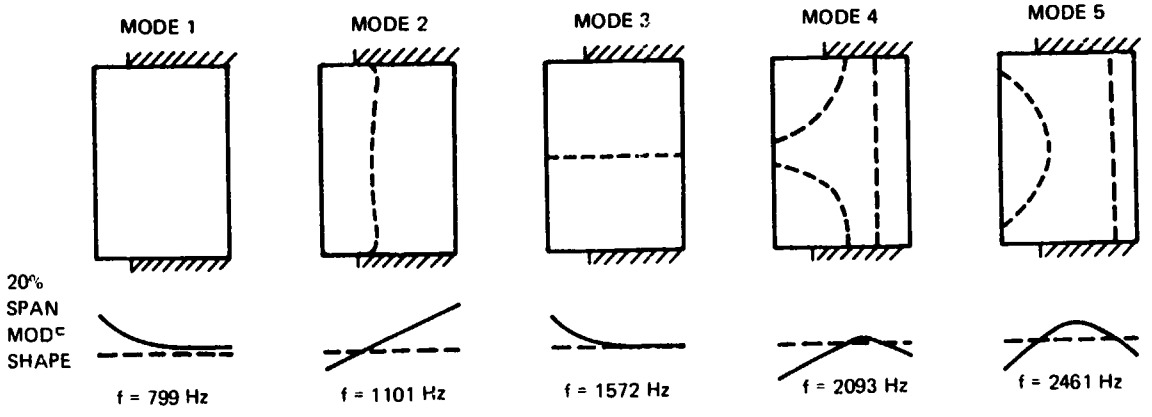

(d)

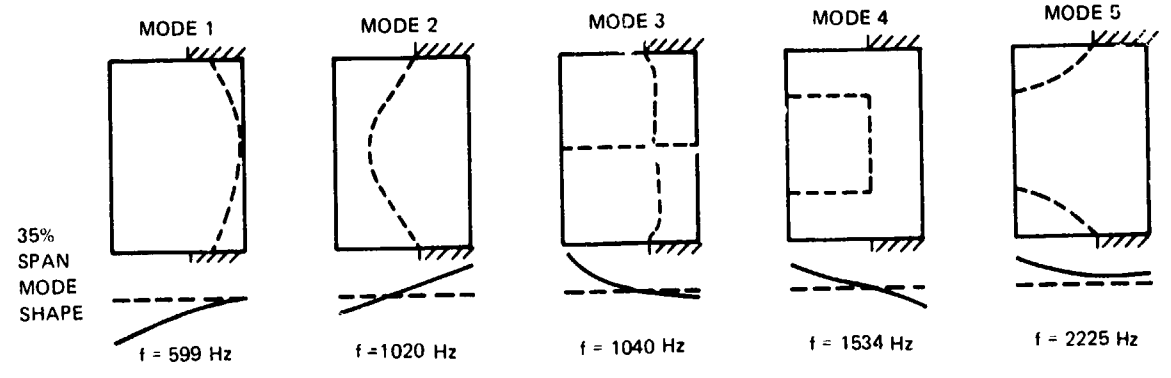

FIGURE 14 (Cont'd) *NASTRAN Results – J-Blade Profile*
(c) 71% Double-Cantilever Attachment
(d) 43% Double-Cantilever Attachment

Following Appendix I, the logarithmic decrement of the motion is given by

$$\delta_{aero} = \frac{W_{aero}}{4\overline{KE}}$$

where KE is the average kinetic energy of the system. The NASTRAN analysis calculates the average kinetic energy of each mode based on the amplitude used to calculate the aerodynamic work.

The modes shown in Figure 14 were analyzed for the following conditions:

Mach number	= 1.65
Speed of sound	= 1000 ft./sec.
Test section pressure	= 5.67 psia
Stagger angle	= 30°
Solidity	= 1.37
Chord	= 3.09 inches
Span	= 4.0 inches

The results of applying the analysis to the modes in Figure 14a-d are shown in Figure 15a-d The aerodynamic damping is plotted against interblade phase angle. The curves that are of most significance are those which exhibit negative values of logarithmic decrement for some range of interblade phase angle. A negative value of δ_{aero} means that the aerodynamic input is excitative; conversely, positive values of δ_{aero} indicate aerodynamic damping. Therefore, in the design of the present experiment large values of negative δ_{aero} are desirable since these improve the chances of flutter.

Figure 15a shows that mode 2 has the highest probability of excitation for the single-cantilever configuration. Since the aerodynamic damping is negative, flutter would be expected to occur in mode 2 for a Mach number of 1.65 provided, of course, the negative aerodynamic input is capable of overcoming the intrinsic damping of blade mode 2. It has been demonstrated under Contract N00019-72-C-0187 (References 1 and 2) that mode 2 for this configuration is indeed unstable. All other modes have positive aerodynamic damping for all interblade phase angles and hence are stable.

Figure 15b shows the aerodynamic logarithmic decrements for the modes of the double-cantilever attachment. For this geometry both the first and second modes show slightly negative aerodynamic damping with the second mode apparently the least stable. The first torsional mode (mode 2) of the double-cantilever blade attachment has a smaller value of δ_{aero} than mode 2 of the single-cantilever attachment partly because of the higher frequency of the double-cantilever attachment. It is interesting to note that the first mode of the double-cantilever attachment, which is capable of inducing a small amount of aerodynamic energy input at zero interblade phase angle, shows evidence of chordwise bending deformation (Figure 15b). Based on these calculations, however, it is unlikely that this blade configuration will flutter.

The results for the 71% double-cantilever attachment are shown in Figure 15c. In this case, mode 2 is again the least stable but, as in the previous configuration, does not have large negative damping.

Figure 15d shows the results of analyzing the 43% double-cantilever attachment. On the basis of δ_{aero} calculations, modes 1 and 4 appear to be equally unstable with large values of negative damping. Each of these modes contain significant amounts of chordwise bending deformation and are therefore likely candidates for chordwise bending flutter.

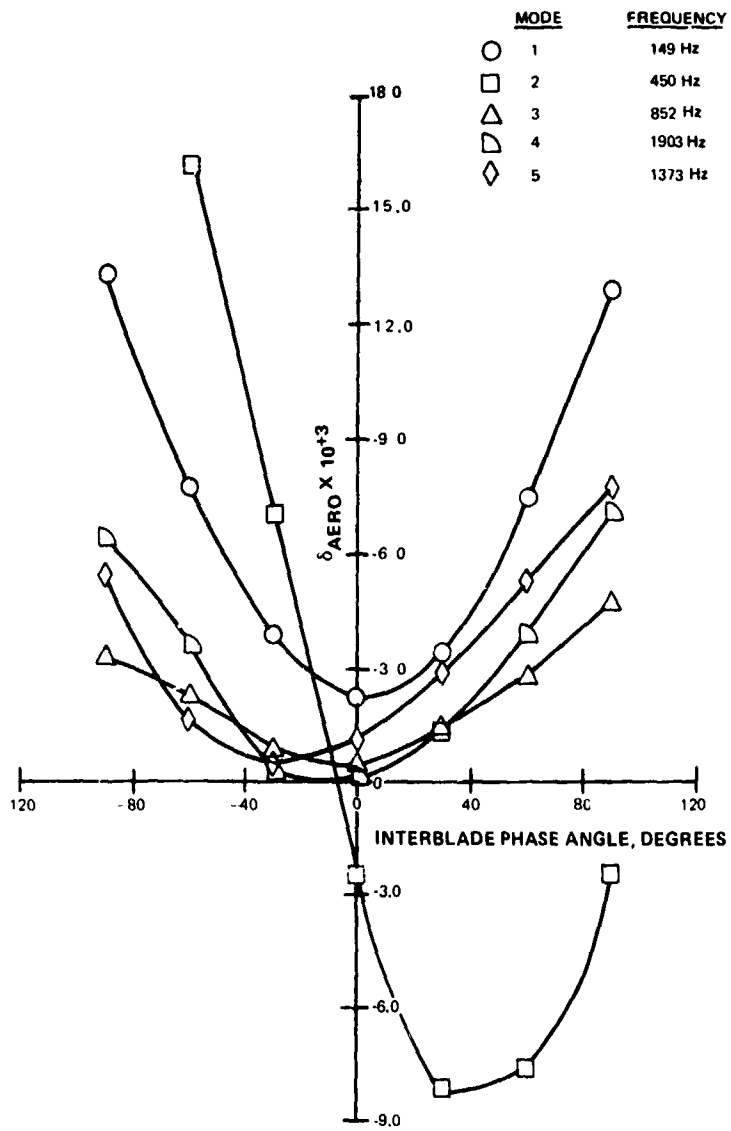

FIGURE 15 *Aerodynamic Damping For First Five Vibrational Modes*
(a) Single-Cantilever Attachment

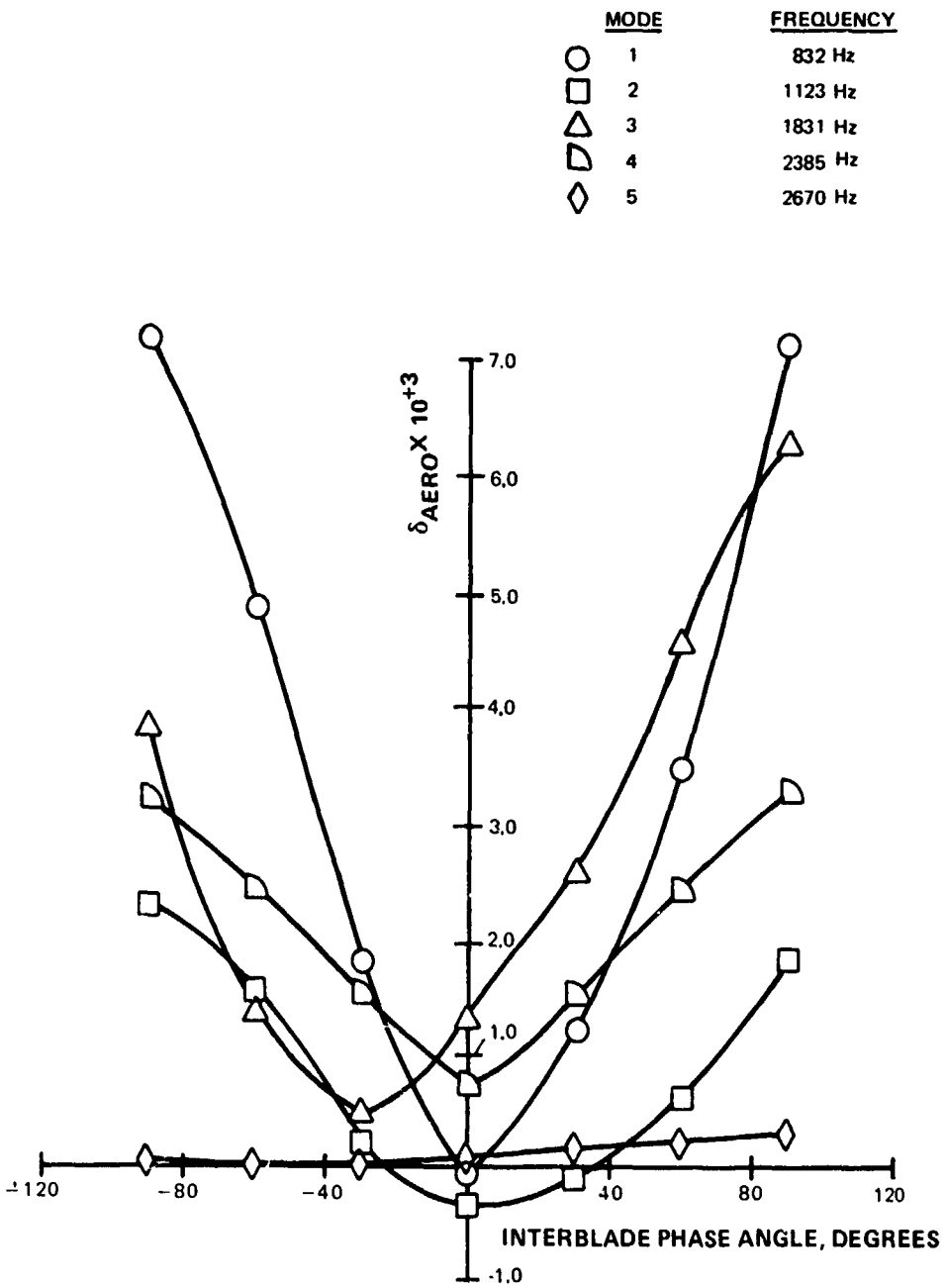

FIGURE 15 (Cont'd) *Aerodynamic Damping For First Five Vibrational Modes*
(b) Double-Cantilever Attachment

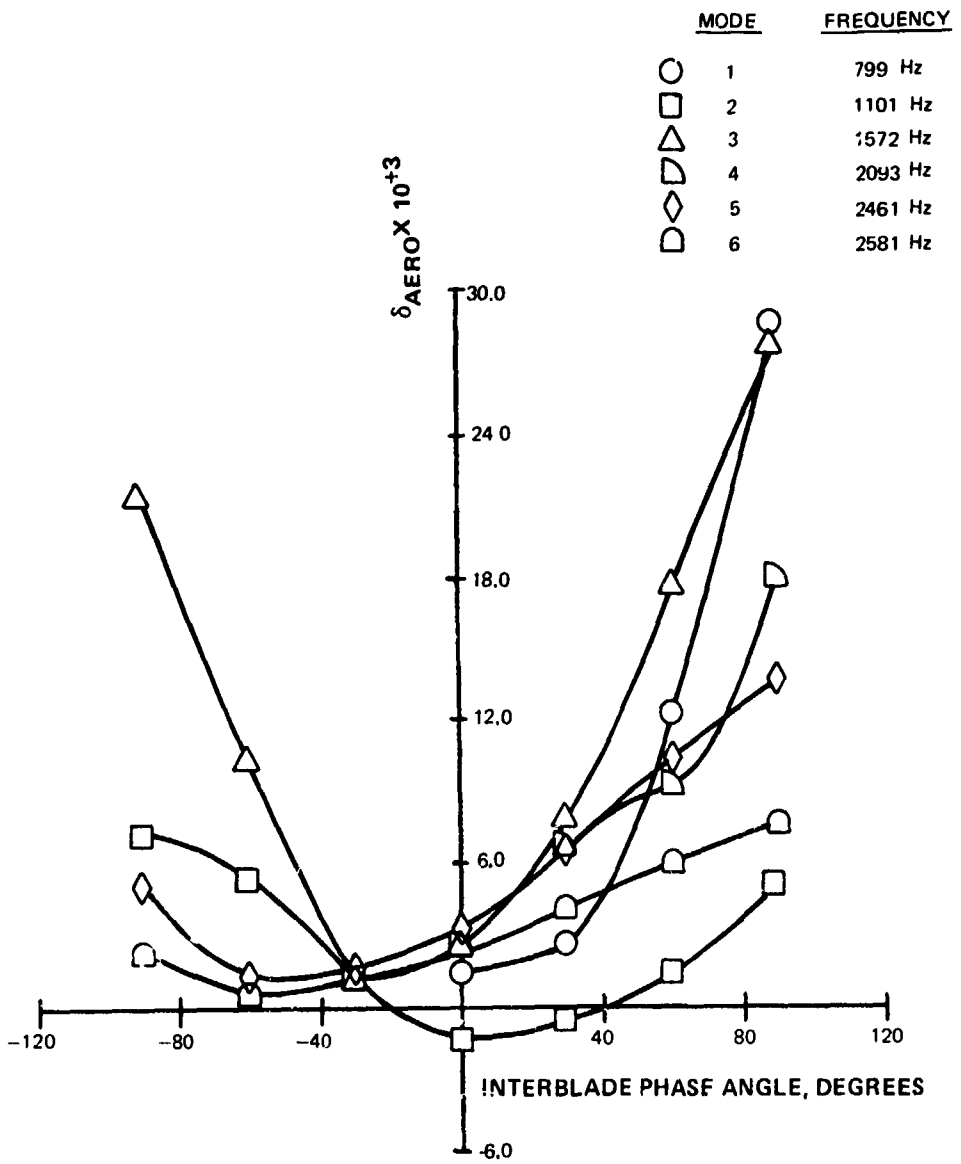

FIGURE 15 (Cont'd) *Aerodynamic Damping For First Five Vibrational Modes*
(c) 71% Double-Cantilever Attachment

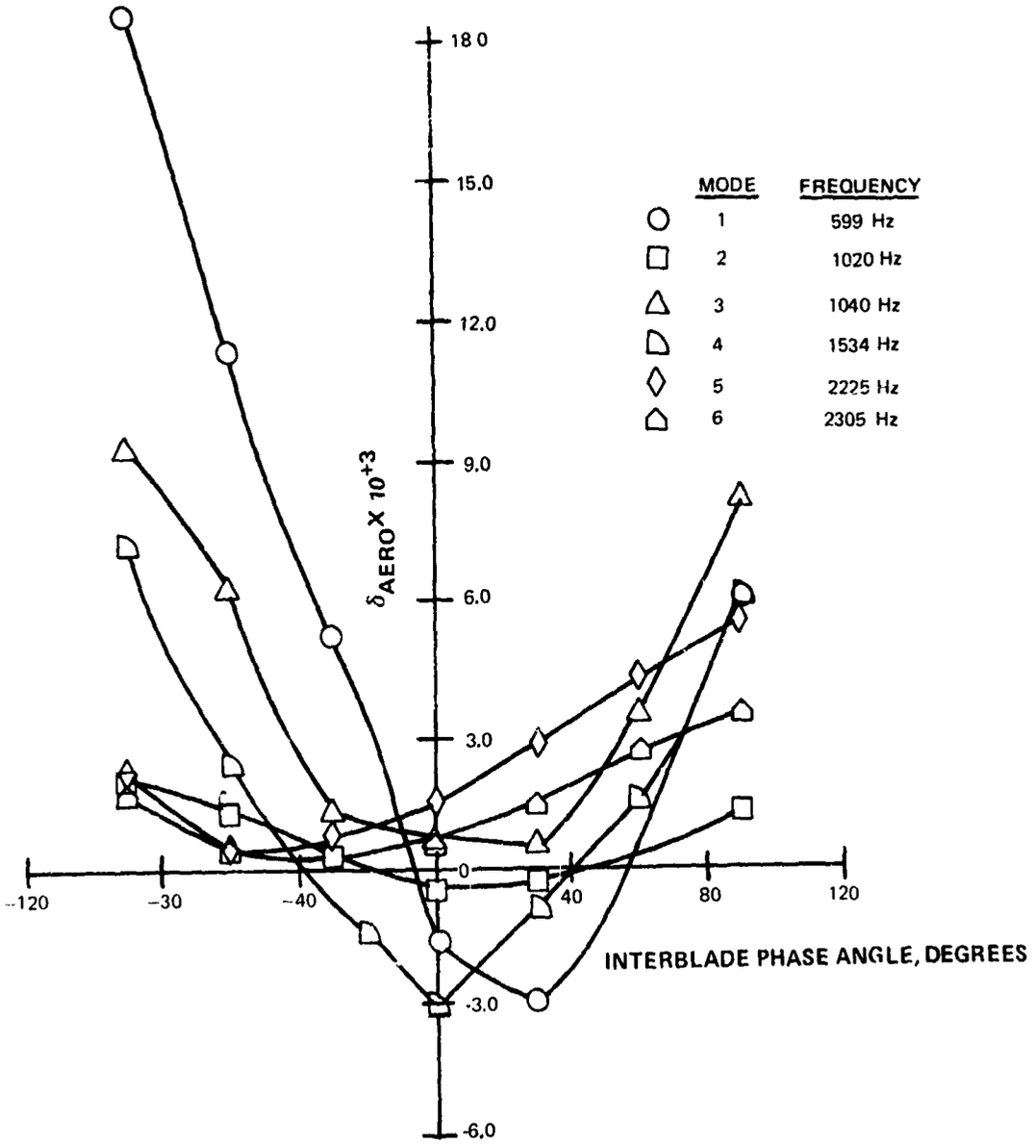

FIGURE 15 (Cont'd) *Aerodynamic Damping For First Five Vibrational Modes*
(d) 43% Double-Cantilever Attachment

APPENDIX III

A. J-BLADE DYNAMICS AND SUPPORT CONFIGURATION

The first series of bench tests were performed using a highly simplified J-Blade prototype, the chordwise profile of which is shown in Figure 16. The prototype was vibration tested as a fully doubly-cantilevered system and as an 80 percent doubly-cantilevered system (cf. Figure 16). Each configuration was tested by recording the natural mode frequencies and associated node line patterns for each mode. The node lines were observed by depositing light weight coarse granules onto the vibrating prototype surface. The results of this test are shown in Figure 16. It is seen that the bench test results are in qualitative agreement with the NASTRAN program results shown in Figure 14 (Appendix II).

The next series of bench tests consisted of recording the first five natural mode shapes and frequencies of each of the five actual test blades. In this phase of the bench test program, holographic equipment was used to obtain greater accuracy and more quantitative information for each mode including its frequency, node-line pattern, logarithmic decrement, and deflection contour map (photographic fringe pattern). Each blade was mounted individually for bench testing using three different support configurations at the tab end: (a) a steel clamp, mounted in a massive support structure, (b) a Lucite clamp identical to (a) with steel shims replaced by Lucite shims, and (c) a tightly fitting slot in a Lucite block, into which the blade tab was bonded with a cyanoacrylate adhesive. In each case, the shank end of each blade was mounted in a steel wedge clamp which simulated the mirrored wall-plate support.

The steel clamping of the tab end was used as a reference condition which closely matched the ideal clamping assumed in the NASTRAN model. The Lucite clamping arrangement was used to simulate the Lucite window support at the tab end. It was found that this attachment is dissipative and does not provide enough rigidity in the support of the tab end. The third configuration, consisting of a tightly fitting slot with no applied loads, proved to be the most satisfactory. In fact, it was found that this technique of mounting the tab end approached the near ideal double-cantilever support that steel clamping provides. The results of these three configuration bench tests are presented next.

B. STEEL CLAMP BENCH TEST RESULTS

Each of the five blades were individually tested with tabs mounted in steel clamps. Holograms of the first five modes of one of these doubly-cantilevered blades are shown in Figure 17. The modes for this attachment can be generally classified as first bending, first torsion, second bending, first chordwise bending, and second torsion. Both the nodal patterns and frequencies of the first five excited modes of the five cascade blades were found to vary from blade to blade. The frequencies are listed in Table III.

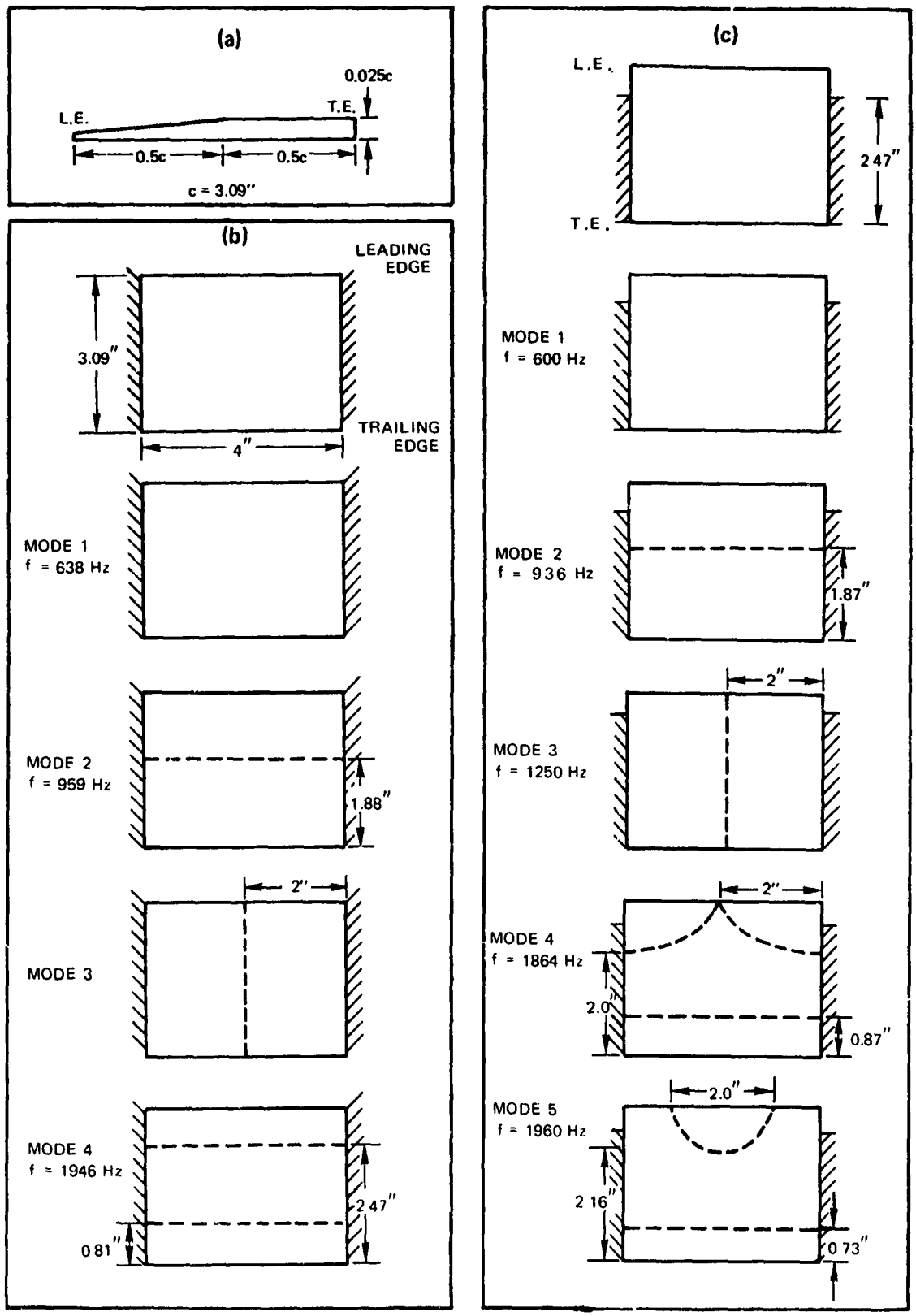

FIGURE 16 *Mode Shapes for J-Blade Prototype*
(a) Prototype Cross-Section
(b) Double-Cantilever Attachment
(c) Partial Double-Cantilever Attachment

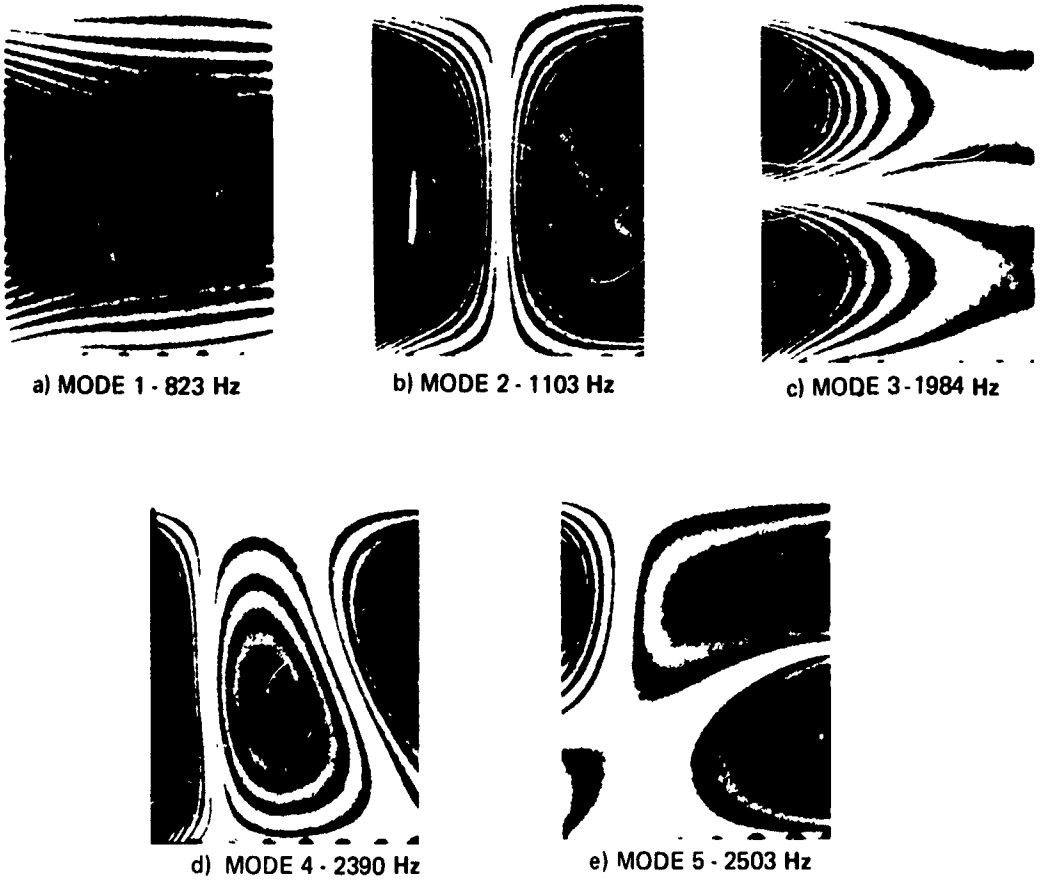

FIGURE 17 *Photographs of Holograms Showing First Five Modes of Blade with Double-Cantilever Attachment*

TABLE III

DOUBLE-CANTILEVER ATTACHMENT BLADE NATURAL FREQUENCIES (STEEL CLAMPING AT TAB END)

Mode	Blade Number 1	2	3	4	5	Average Frequency
1	743	834	780	825	766 Hz	790
2	1062	1134	1093	1140	1080	1102
3	1792	1931	1863	1913	1801	1860
4	2412	2452	2394	2476	2352	2417
5	2427	2592	2450	2608	2430	2502

The variation in the mode frequencies from blade to blade was initially attributed to a combination of two effects, namely, nonuniformities in blade thickness in the spanwise direction, and irregularities in the dimensions and attachment of the blade tabs. It is possible, however, to immediately eliminate one of these effects as being of primary importance by noticing the relative lack of variation in the frequencies of modes 2 and 4 as compared to modes 1, 3, and 5. Modes 2 and 4 are essentially free-plate modes and so are inherently insensitive to variations in the method of blade support. Their behavior is largely a function of the construction of the blade itself; that is, they are a function of the blade mass distribution. Therefore, the relative lack of variation in the frequency of modes 2 and 4 implies that blade nonuniformity effects are of secondary importance for these test blades. Conversely, modes 1, 3, and 5 show the greatest variation in frequency from blade to blade, and since these modes are largely governed by the method of support, their variation would indicate a need to render the tab end support more uniform from blade to blade. Finally, corrections due to blade nonuniformity can be made by applying the tuning process described in Appendix V.

The comparison between the holograms of the various blades (e.g., Figure 17) and the NASTRAN outputs are in general agreement with respect to both frequency and mode shape. Table IV shows the frequency comparison. The modes which are least sensitive to the end attachments (torsion mode 2 and chordwise bending mode 4) are predicted best with NASTRAN in which ideal clamping (rigidly fixed) is assumed. This is reasonable since modes 2 and 4 are relatively insensitive to the support configuration.

TABLE IV

COMPARISON OF STEEL CLAMP EXPERIMENTAL AND THEORETICAL RESULTS

	Mode 1	Mode 2	Mode 3	Mode 4	Mode 5
Average of 5 blades (Hz)	790	1102	1860	2417	2502
NASTRAN (Hz)	832	1123	1831	2385	2670

The experimentally and analytically determined mode shapes for the first five modes are shown in Figure 18. The agreement is the poorest for the first mode where the predicted and observed behavior of the trailing edge portion of the blade is different.

From Figure 18, it is seen that there is little difference in the mode shapes for the second mode (torsion) where the position of the twist axis is the most important feature of the mode. The third and fifth modes are both fairly well modeled by the NASTRAN program while the fourth mode (chordwise bending) results are in excellent agreement. The overall conclusion is that NASTRAN calculations can be reliably used to predict the natural frequencies and mode shapes of the test blades, especially in the torsion and chordwise modes.

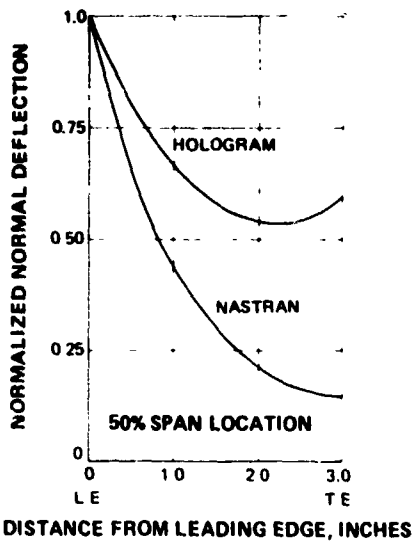

a) MODE 1

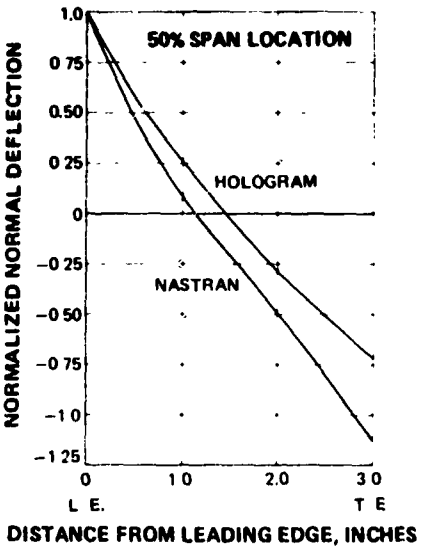

b) MODE 2

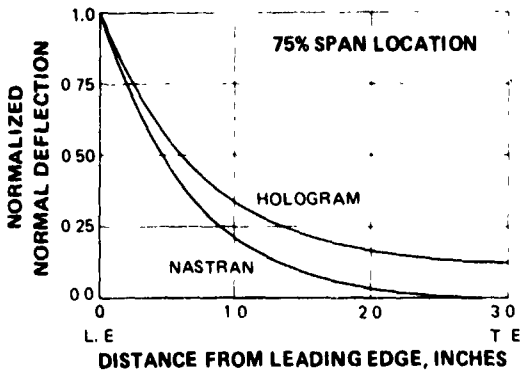

c) MODE 3

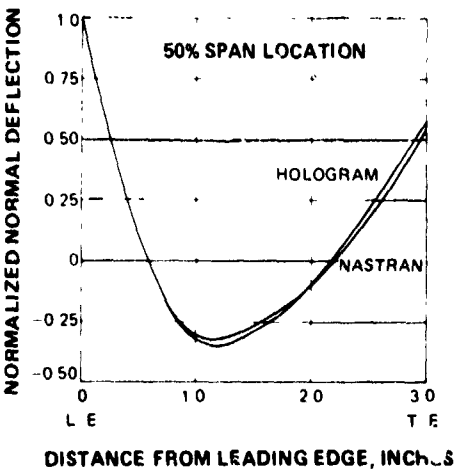

d) MODE 4

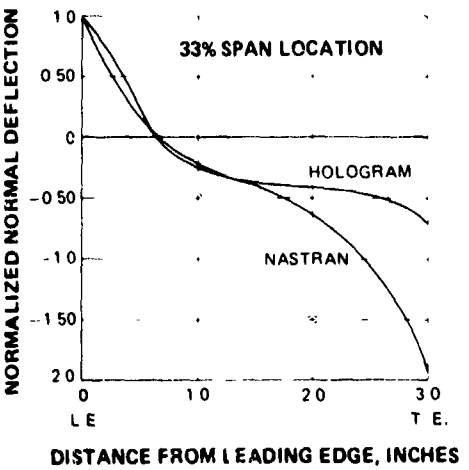

e) MODE 5

FIGURE 18 Hologram and NASTRAN Mode Shape Comparison

C LUCITE CLAMP BENCH TEST RESULTS

In order to duplicate the structural environment of the tunnel more closely, a follow-up bench test was carried out by replacing the steel clamp at the blade end tab with a Lucite clamp to simulate the Lucite window support of the tunnel during actual aerodynamic testing. Because of the characteristics of the Lucite material, this support arrangement was found to increase the system damping and also resulted in a significant deterioration in the stiffness of the blade support at the tab end. The loss of vibration energy was due to shear stress losses in the Lucite caused by clamping. The following table of modal frequencies of one blade depicts the resulting differences that were obtained between clamping configurations. (Figure 19 shows the accompanying ideal flat-plate node lines for each of these modes.) It is noted that modes 1, 3, and 5, which are strongly dependent on boundary conditions, suffered a general decrease in frequency from steel clamp to Lucite clamp. This is due to the lower stiffness of the Lucite clamp arrangement. It is further noted, however, that modes 2 and 4 were not significantly affected by the change, thus reinforcing the premise that these modes are primarily free-plate modes.

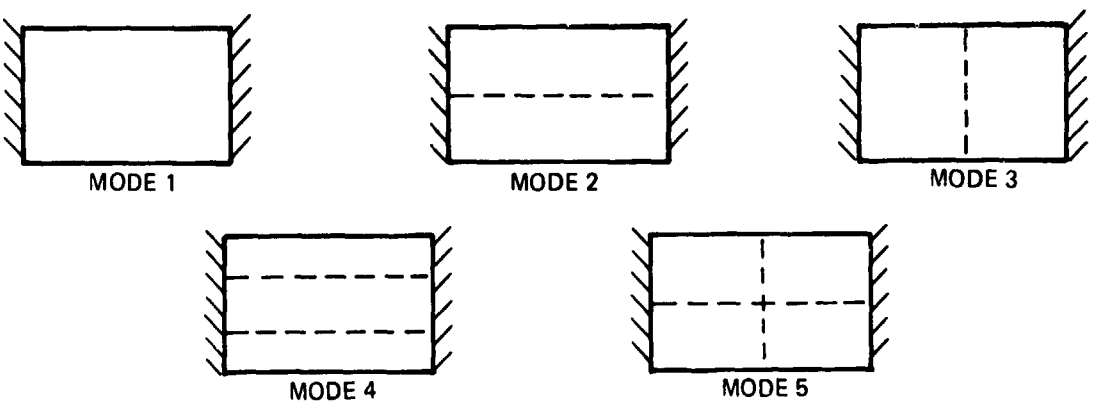

FIGURE 19 Schematic Diagrams of Node Lines for First Five Modes

A further examination of the frequency data in Table V shows that this 'soft' support configuration caused mode 5 to drop enough in frequency to cause a shift in the position of modes 4 and 5 in the frequency hierarchy. Because of this, even though the frequency of mode 4 did not change significantly during this shift, its mode shape did. Figures 20a and 20b show this effect schematically. This change in the nodal patterns of modes 4 and 5 occurs because they are near neighbors, as their frequencies indicate, and are therefore subject to the phenomenon of mode admixture (Ref. 8); that is, they are interdependent.

Therefore, because of the increase in system damping, the lower stiffness at the tab end, and the complications arising from an interchange in the position of modes 4 and 5 in the frequency spectrum, the Lucite clamping arrangement was abandoned.

TABLE V

BLADE FREQUENCY FOR TWO ATTACHMENT MATERIALS

Mode	Steel Clamp (Blade 3)	Lucite Clamp (Blade 3)
1	780 Hz	719
2	1093	1039
3	1863	1757
4	2394	2379
5	2450	2331

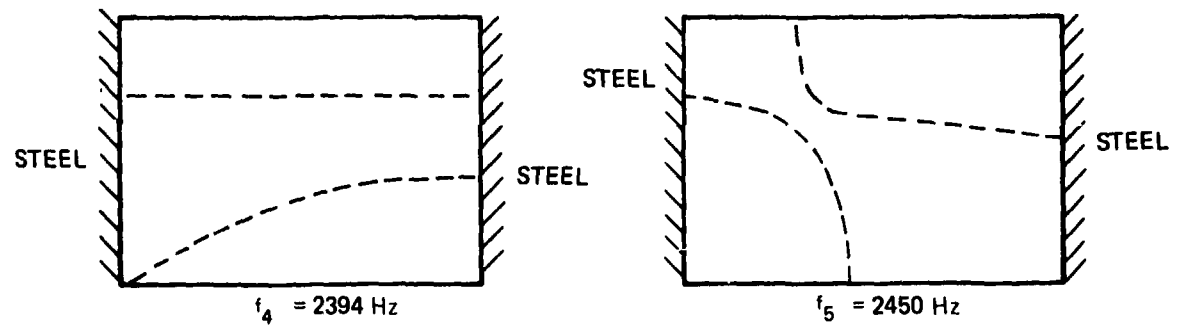

(a) STEEL ($f_4 < f_5$)

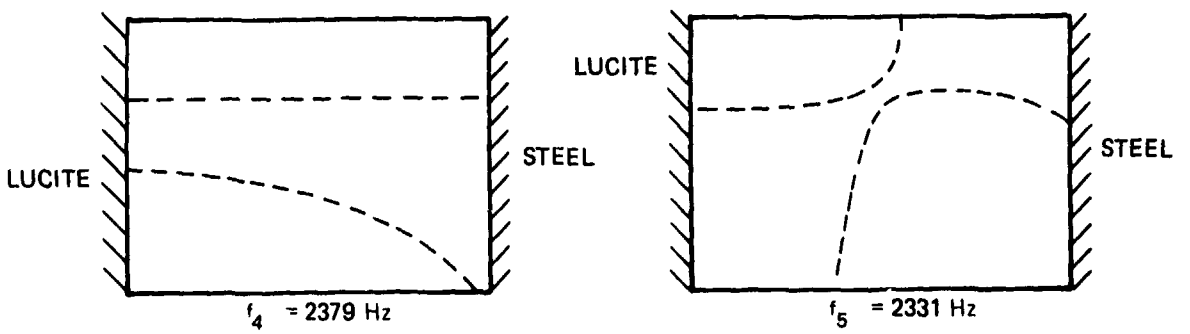

(b) LUCITE ($f_4 > f_5$)

FIGURE 20 Effect of Attachment Material on Mode Shape

D. LUCITE SLOT SUPPORT RESULTS

The results presented thus far indicate a need to improve the Lucite window support and to obtain uniform interblade mode shapes and frequencies for the modes of interest. Three problems, associated with interblade discrepancies, have been cited. Two of these problems are related to the variation in frequency and mode shape of the individual modes from blade to blade. This variation was attributed to nonuniform mass distribution and varying conditions at the tab end support of each blade. The third problem was identified with the admixture of modes 4 and 5 which causes these modes to be very sensitive to slight variations at the tab end support. (This can be seen, for example, in Figure 17b.)

The effects of blade nonuniformities, already shown to be of secondary importance, were ignored until the blade tuning phase of this program took place (Appendix V). The elimination of mode admixture effects required that the blade geometry be altered to separate these modes such that the mode 4 nodal pattern would be insensitive to variations at the tab end. This was achieved by introducing spanwise grooves in the midchord region and is discussed in Appendix IV. Prior to the next series of bench tests (Lucite slot configuration), the variations in blade dynamic response associated with blade tab nonuniformities was corrected.

Measures were taken to begin reducing interblade differences by standardizing the end tabs to a common size through minor machining. The blade end-tabs were all machined to a uniform thickness of 0.0625 inches, corresponding to the size of the tool used for machining the slots in the Lucite window. This technique ensured a snug fit of the tabs in their respective mating Lucite slots while, at the same time, reducing the variation of the mounting conditions at the window support.

The mounting conditions of the individual blades at the window end were duplicated during the bench tests by constructing five Lucite blocks into which 0.0625-inch slots were machined for blade tab insertion. Figure 21 shows the front view of a typical one-inch thick slotted Lucite block (same thickness as Lucite window). In agreement with the actual wind tunnel setup, no clamping was applied normal to the blade tabs as in the previous series of bench tests. In the slot of Figure 21 are shown three small circular holes into which a cyanoacrylate bonding agent was injected via hypodermic needles after the blade tabs were properly inserted. The integrity and repeatability of the mounting of the individual blades into their respective Lucite block slots were then tested. It was found that this support allowed a partial recovery of the cantilever support originally provided by the steel-shim-clamp configuration. Therefore, the snug-fitting tabs in Lucite slots in combination with cyanoacrylate bonding provides enough stiffness at that end of the blade to consider it nearly an ideal cantilever support. This situation is convenient in that reliable analysis comparisons can be made via the NASTRAN program.

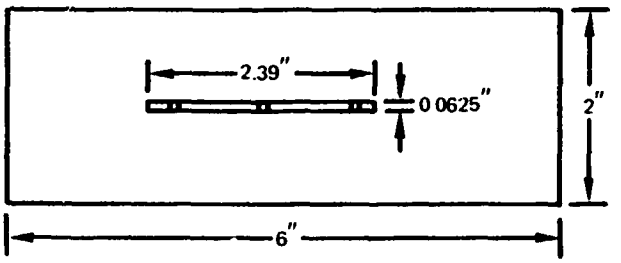

FIGURE 21 Slotted Lucite Block Arrangement

The repeatability of the blade response was verified by dismounting and remounting the blades in the same way and by interchanging the Lucite blocks. Table VI shows the results for the first five modes of blade 3 when supported in steel clamps, Lucite clamps, and when glued into Lucite slots with a repeatability check (note the insensitivity of free-plate modes 2 and 4). Also included are the NASTRAN program outputs for comparison.

An important outcome of this new method of support with uniform blade tabs was a significant reduction in the degree of variation in the mode frequencies from blade to blade. It is noted, however, that modes 4 and 5 continue to be near neighbors thus indicating that mode admixture is still a problem.

TABLE VI

COMPARISON OF BLADE 3 FREQUENCIES FOR VARIOUS ATTACHMENTS
(Frequency, Hz)

Mode	Steel Clamp	Lucite Clamp	Glue	Repeat	NASTRAN
1	780	719	798	799	832
2	1093	1039	1085	1088	1123
3	1863	1757	1900	1919	1831
4	2394	2379	2386	2394	2385
5	2450	2331	2424	2424	2670

APPENDIX IV

MODIFICATIONS OF BLADE GEOMETRY

A. EMERGENCE OF MODE 1 AS PRIMARY MODE OF INTEREST

As described in the main text of this report, mode 4 was the initial chordwise flutter mode of primary interest. Because of this, two interrelated problems had to be resolved: (a) separating modes 4 and 5 to avoid intermodal interference, and (b) lowering the mode 4 frequency enough to significantly increase the possibility of aerodynamic excitation in that mode. It was predicted that the removal of material from the blade midchord region in the form of a spanwise groove would be the most effective way of achieving both objectives.

The proposed technique was to remove material from the midchord region until the frequency of the mode (mode 4) dropped low enough to ensure the occurrence of flutter. However, before cutting into the actual test blades, it was shown by NASTRAN analysis and by a supporting experiment using a prototype blade that the mode 4 frequency drops more than the remaining mode frequencies if the material is removed from near the 40% chord position measured from the leading edge.

Four airfoil configurations were analyzed with the NASTRAN finite element program, including both the fully double-cantilevered and 43% double-cantilevered configurations with and without a spanwise groove. For the cases containing a spanwise groove, it was assumed in the NASTRAN model that the density of that part of the blade from which material was removed was increased to account for the addition of a low strength, high density filler. The depth of the spanwise cut assumed in the NASTRAN model was one-half the chord thickness in the region between 1.2 inches and 1.8 inches from the leading edge. The cut is shown schematically in Figure 22. Table VII summarizes the NASTRAN program results, including a calculation of the aerodynamic logarithmic decrement for each mode.

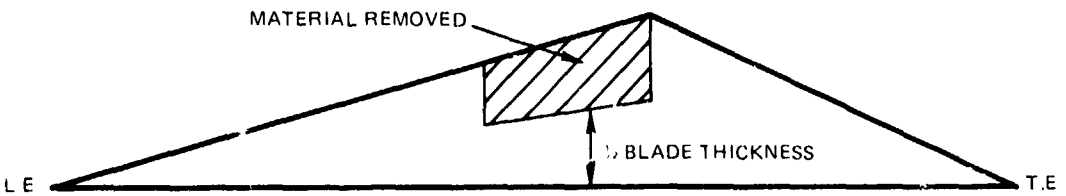

FIGURE 22 Chordwise Section Showing Idealized NASTRAN Cut

TABLE VII
GROOVED PROTOTYPE VIBRATION TEST IN LUCITE BLOCK

	Frequency	Logarithmic Decrement
UNFILLED	299	0.0109
EPOXY-FILLED	317	0.0220
RTV-FILLED	300	0.0108

A comparison of configurations A and C from Table VII shows that the spanwise cut reduces all of the individual mode frequencies, but by varying amounts. The frequencies of these modes were calculated to be lowered by 11.7%, 6.6%, 10.9%, 23.5%, and 3.2%, respectively. An encouraging outcome of this is the successful significant lowering of the mode 4 frequency as compared with that of mode 5 thus causing these two modes to separate. In addition, it is seen that the aerodynamic input into modes 1, 2, and 4 increased, therefore improving the chances of obtaining flutter in the chordwise bending mode 4.

When the spanwise cut was introduced into the 43% double-cantilevered blade, the NASTRAN predictions showed a significant amount of chordwise bending in both modes 1 and 4. In fact, there is enough deformation in mode 1 to rival that of mode 4 and, moreover, subsequent aerodynamic calculations show that mode 1 is capable of inducing a much larger aerodynamic input. Emphasis of this experimental program was therefore shifted toward mode 1 of the grooved, 43 percent doubly-cantilevered blade configuration.

C. EVALUATION OF EPOXY-FILLED BLADE GROOVES

As described in the text of this report, this system failed to flutter for both Mach 1.31 and 1.65 conditions. A post-experiment examination of the blades was carried out before disassembling the blades from the window and mirrored wall-plate. It was initially observed that some of the dense epoxy in the midchord region had broken away during the Mach 1.65 flutter test. (A previous inspection of the blades after the Mach 1.31 test had shown no loss of the midchord filler.) The primary consequence of this was the altered aerodynamic shape of the blades in that region. The post-experiment blade frequencies were measured for blades 1 to 5 and found to be 398 Hz, 395 Hz, 423 Hz, 395 Hz, and 381 Hz, respectively. The reduction in the frequencies was due to the deterioration of the blade support at the window end due to blade buffeting at high backpressure during the Mach 1.65 test. The corresponding logarithmic decrements were also measured and found to be 0.022, 0.016 0.020, 0.015, and 0.020, respectively. Comparing these values with the logarithmic decrement of the aerodynamic input, $\delta_{aero} = -0.016$ as determined earlier in this Appendix (Table VII, case D), the immediate indication of the theory is that, on an individual basis, these blades were only marginally stable at M = 1.65. Figure 5b illustrates the high sensitivity of δ_{aero} to slight variations in reduced frequency for the mode 1 response of the 43% double-cantilever attachment containing no spanwise groove. From this graph, it can be safely deduced that the present configuration behaves in much the same way.

In order to determine what effect the plastic steel had on the blade behavior, all of the blades were scraped clean of epoxy, and the frequencies measured once again with the blades still assembled to the window and mirrored wall-plate. The new frequencies for blades 1 to 5 were 358 Hz, 383 Hz, 406 Hz, 387 Hz, and 379 Hz; that is, the epoxy had caused a mean increase of 4 percent in the blade frequencies relative to the grooved, unfilled configuration. Furthermore, the individual blade damping coefficients were lower. Consequently, the plastic steel epoxy, used to fill the spanwise grooves, was detrimental to flutter since it helped to stabilize the blades by increasing both the intrinsic damping and frequency of each blade.

C. RTV-FILLED SPANWISE GROOVE CONFIGURATION WITH SPANWISE CUTS: THE FINAL FLUTTER MODEL

Because the steel epoxy was determined to be detrimental to the objectives of this program, another material for filling the spanwise grooves was introduced. This material was RTV (a silicon rubber sealer). A grooved prototype test was carried out in which the chordwise support was cut back 57%. The prototype was vibration tested with: (a) no filler, (b) epoxy filler, and (c) RTV filler. The results of this test appear in Table VII. Clearly, the epoxy substance is the inferior filler between the two. The original reason for choosing the dense epoxy was to recover most of the blade mass that was removed for the purpose of further weakening the midchord region. This, however, was abandoned in favor of RTV which had little or no influence on either the blade damping or the frequency.

B. DENSE EPOXY-FILLED SPANWISE GROOVE CONFIGURATION AND ITS FAILURE TO FLUTTER

Before proceeding directly to the actual blade hardware, a prototype blade was fabricated to help verify the results of the NASTRAN program predictions, especially with respect to changes in mode 1 in moving from configuration A to configuration D of Table VII. The changes consisted of cutting the prototype back 57% along the chord at each span end from the leading edge and then removing material from the prototype midchord region and replacing this material with a dense epoxy filler. The prototype was tested by mounting it in the same way that the actual blades were mounted in the final bench test described in Appendix III; that is, it was supported by a steel clamp at one span end and glued into a Lucite slot at the other end. The frequencies of the first five modes were recorded as 695 Hz, 890 Hz, 1695 Hz, 1916 Hz, and 2078 Hz, where old modes 4 and 5 were shifted in the frequency hierarchy; that is, mode 4 had a frequency of 2078 Hz and mode 5 was at 1916 Hz. After cutting the chordwise supports back 57%, material was removed along the prototype midchord as shown in Figure 23. The filler was Devcon plastic steel, which is an epoxy having a density of approximately 70% the density of the steel blades. The new mode 1 frequency was measured at 317 Hz which is a 54% decrease in the original mode 1 frequency. This compares well with the 46% decrease in the mode 1 frequency from the NASTRAN predictions in going from configuration A to configuration D (Table VII).

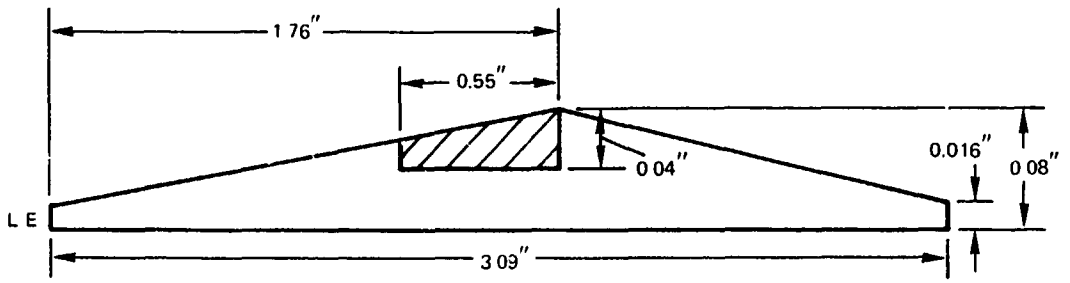

FIGURE 23 Chordwise Section of Actual Prototype with Spanwise Groove

Based on these results, the actual test blades were altered accordingly to enhance mode 1 excitation. The plan view of the altered test blades is shown in Figure 24. The actual chordwise cut left a 37% double-cantilever which consisted of a 57% removal of the chordwise support at the forward end and a 6% removal at the trailing portion. The midspan groove was located on the suction side of the blades. After filling the groove with plastic steel, the mode 1 frequencies for blades 1 to 5 were measured at 469 Hz, 466 Hz, 437 Hz, 442 Hz, and 435 Hz. These frequencies were obtained with the tab ends of the blades individually mounted into their respective Lucite slots and bonded with cyanoacrylate glue. These blades were subsequently rough-tuned to a target frequency of 435 Hz and then mounted in cascade between the mirrored wall-plate and Lucite window for final tuning. The final blade pack frequency was 423.4 Hz ± 0.4 Hz. (The details of tuning are presented in Appendix V.) A blade to blade frequency variation of less than ±2% is desirable since unsteady aerodynamic analysis assumes uniform frequency. Furthermore, experience has shown that a detuned system tends to be more stable than a tuned system.

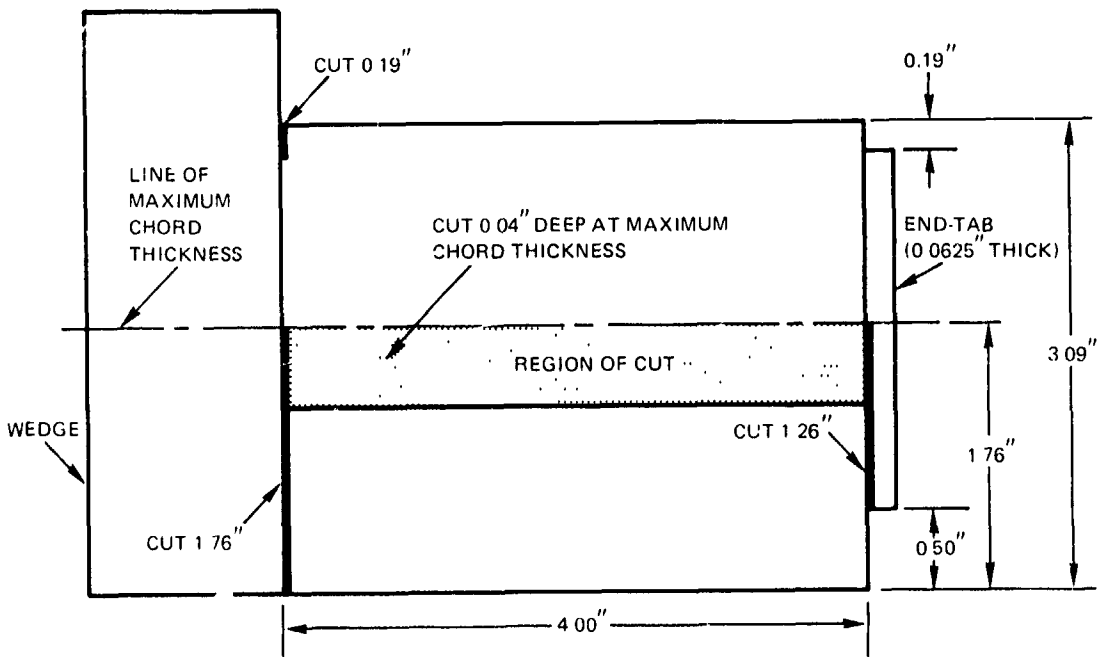

FIGURE 24 Plan View of Actual Test Blade Showing Chordwise Cuts and Spanwise Grooves

To further improve the chances for flutter, a decision was made to again lower the mode 1 frequency, but in such a way as to retain the existing double-cantilever attachment. This was done with the belief that the nominal 5 percent drop in frequency caused by a change in filler substance would not be enough to ensure flutter, especially, since no evidence of flutter tendency was perceived in the epoxy-filled configuration test. Spanwise cuts, such as those shown schematically in Figure 7, were therefore introduced into the blade geometry. Initial experiments to this end were carried out using the prototype to evaluate the effectiveness of this technique both with respect to changes in the frequency and the logarithmic decrement. This experiment was carried out with the prototype supported as a double-cantilever with steel clamps at both ends and with the spanwise cuts at either end being equal. Table VIII shows the results of this test. It is seen that this approach achieves the results that are desired in terms of the reduction trend in both frequency and logarithmic decrement. In order to compare this result with the Lucite block support results (Table VII), the 0.6-inch spanwise cut prototype filled with RTV was mounted in a Lucite block and vibration tested. The frequency was 257 Hz and the logarithmic decrement became 0.0055. This is an encouraging improvement when compared with Table VII values of $f = 300$ Hz and $\delta = 0.0108$ for no spanwise cut.

TABLE VIII
FREQUENCY-LOWERING EXPERIMENTAL RESULTS
FOR THE PROTOTYPE IN STEEL CLAMPS

Spanwise Cut	Frequency	Logarithmic Decrement
0.0"	298 Hz	0.0075
0.4"	271 Hz	0.0043
0.6"	255 Hz	0.0028

Finally, from Table VIII, it is seen that the 0.4-inch spanwise cut produced a 10 percent drop in frequency. This was judged to be a sufficient reduction in the frequency of the actual blades. Upon filling the spanwise grooves of the blades with RTV and cutting the blades 0.4-inches in the spanwise direction as in Figure 7, the blades were individually rough-tuned to a target frequency and then mounted in cascade to the mirrored wall-plate and Lucite window for final tuning to a common interblade frequency of 360 Hz. Details of this procedure are presented in the next appendix.

APPENDIX V

BLADE TUNING

Before tuning the blade hardware, effects of minor extensions of the chordwise cuts on the prototype blade were tested with respect to both aligning the node line and lowering the frequency of mode 1. It was found that a 0.08-inch adjustment at one span end noticeably altered the node line pattern. It was also determined that a 0.04-inch extension of the chordwise cut at each span end reduced the prototype mode 1 frequency by 4 Hz. Based on these results, it was decided to tune the blades by slight extensions of the chordwise cuts for the epoxy-filled configuration.

Since the lowest recorded frequency was 435 Hz for blade 5 (see Appendix IV for the epoxy-filled system), the five-blade system was made more uniform by individually rough-tuning the remaining blades to a common frequency of 435 Hz. Because there was no way of guaranteeing that this interblade frequency could be retained after dismantling the blades from their individual Lucite blocks and then remounting them in cascade in the Lucite wind tunnel window, two interrelated requirements became evident: a) the blades had to be fine-tuned in their tunnel-mounted configuration (wall-plate, cascade, and window intact), and 2) this tuning had to be accomplished outside the tunnel test section. To fulfill these requirements, the window mounting frame of the wind tunnel was modified to accept the installation of a completely mounted unit package consisting of the window, the cascade, and the mirrored wall-plate.

The instrumented blades were subsequently mounted in cascade to the wall plate and Lucite window. The resulting package was then secured to a rigid frame constructed of 3/4-inch aluminum plate (Figure 25). This last step ensured a proper simulation of the massive tunnel wall support of both the window and wall-plate, and guaranteed the desired double-cantilevering of the blade pack during the bench test.

Before fine-tuning the cascade, the individual mode 1 frequencies of blades 1 to 5 were recorded at 394 Hz, 411 Hz, 423 Hz, 425 Hz, and 428 Hz, respectively. The discrepancy between these frequencies and the common value of 435 Hz achieved previously by rough tuning illustrates the reason why final tuning should be carried out with the blades mounted in the final test rig. The blades were fine-tuned to a mean frequency of 423.4 Hz (± 0.4 Hz). Blades 1 and 2 were tuned upward in frequency by extending the chordwise supports with small amounts of epoxy at each span end. The nature and location of this epoxy was such that its effect as a blade damper was negligible. The frequency of blade 3 was left unaltered while the frequencies of blades 4 and 5 were tuned downward by filing away small amounts of blade material along the chordwise supports.

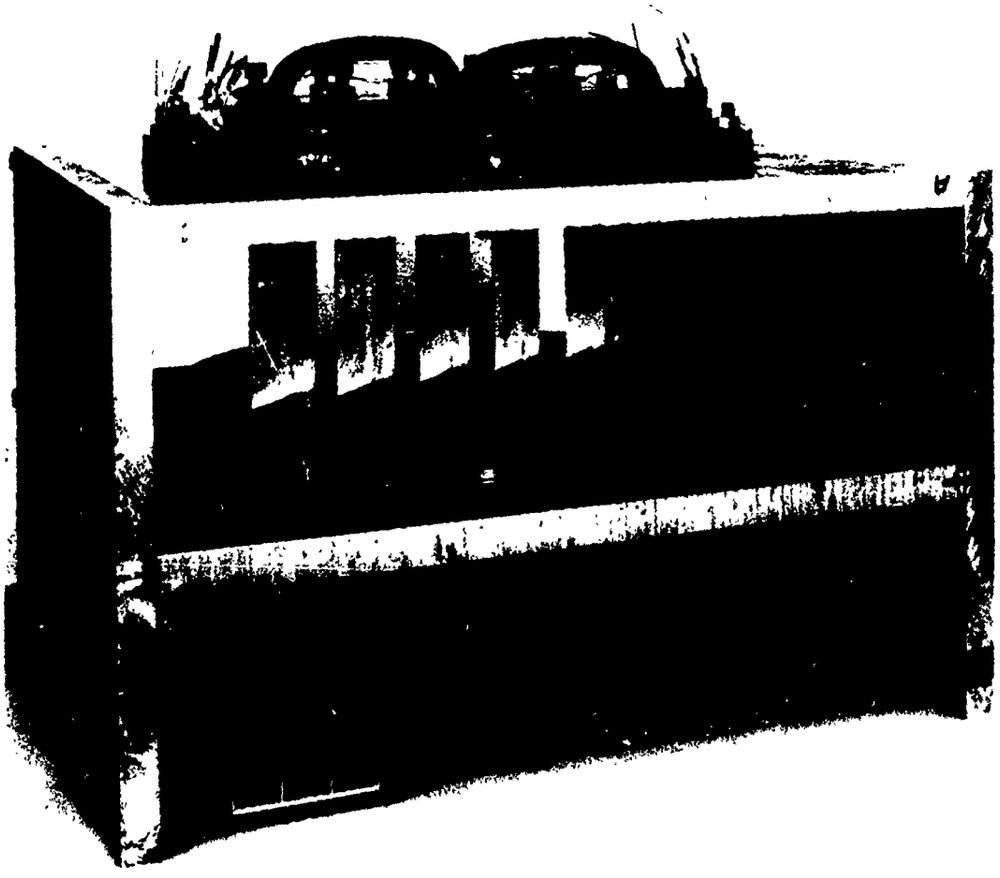

FIGURE 25 Photograph of Blade Pack in Rigid Bench-Test Frame

During the process of bolting the window to the tunnel wall frame, two of the blades were inadvertently detuned as the bolts were tightened. The amount of detuning, however, was only slight. This problem of window securement to the wind tunnel wall was rectified for the subsequent flutter test of the cascade configuration containing RTV in the grooves by relieving the close tolerance between the frame and the tunnel wall and introducing a soft rubber gasket to prevent unwanted pretest stresses at the window end of the cascade. As described in the text of this report, this configuration failed to flutter for reasons given in Appendix IV.

As described in the last part of Appendix IV, prototype tests showed that 0.4-inch spanwise cuts at both span ends (Figure 24) produce a 10% drop in the frequency of mode 1, and this was judged to be a sufficient reduction to ensure flutter in the chordwise bending mode. The RTV-filled blades were cut accordingly. The exact location of the cuts were coincident with the aft edge of the spanwise groove. In using the same mounting configuration as described earlier (Figure 25), the frequencies of blades 1 to 5 were measured to be 350.3 Hz, 359.6 Hz, 383.7 Hz, 366.7 Hz, and 346.7 Hz. (Rough-tuning in this case had been bypassed.) The corresponding logarithmic decrements were determined to be 0.0117, 0.0115, 0.0124, 0.0107, and 0.0200, respectively.

Because of its high intrinsic damping, blade 5 was not tuned and, consequently, left at $f = 346.7$ Hz and $\delta = 0.0200$. The rest of the blades were tuned to the lowest frequency of the remaining four blades. Tuning was achieved by slightly extending the spanwise cuts symmetrically until the desired blade frequencies were reached. The tuned frequencies of blades 1 to 4 became 359.3 Hz, 359.0 Hz, 360.0 Hz, and 359.7 Hz, while δ was determined for each blade to be 0.0085, 0.0110, 0.0101, and 0.0105, respectively. Finally, in order to avoid the generation of shocks at, or flow leakage through, the spanwise cuts, the cuts were filled with RTV hence recovering the original local aerodynamic blade shapes. The cascade package was then installed into the wind tunnel for a successful Mach 1.65 flutter test.

APPENDIX VI

NONLINEAR VIBRATION BEHAVIOR OF CRACKED BLADES

It was pointed out in the main text of this report that the blade pack fluttered with a mean frequency of about 245 Hz, which is considerably lower than the frequency to which the blade pack was tuned before the flutter test began. Effects due to aerodynamic loading and blade thermal expansion were immediately eliminated as possible causes for such a large drop in cascade frequency. A visual examination of the individual blades was made, and it was found that blades 1, 2, and 3 had sustained significant fatigue damage in the form of noticeable spanwise cracks near the blade midchord, as described in this report. From these observations, it would appear that the cracks might help explain the severe drop in the frequency of the cascade oscillations during the Mach 1.65 flutter test. This is especially true of blades 1 and 3, since these blades appear to have been the most severely damaged of the five blade system.

By following the same procedure used in previous bench tests, a post-experiment bench test was carried out to determine the frequencies of the damaged blades. As before, this procedure employed very small amplitude excitation. Table IX lists the frequencies before and after the flutter test. Following this, a higher amplitude excitation was imposed on the blades, and the results are also listed in Table IX. Although the post experimental frequency response test showed no blades having a natural frequency of 245 Hz at low-amplitude resonance excitation, the frequency-drop trend for the blades seems to agree qualitatively with what might be expected from the physical condition of the blades. A possible explanation of why a discrepancy exists between the flutter test and small-amplitude bench test results is that the effective stiffness of the cracked blades decreases with the amplitude of vibration, even if the crack is nonpropagating. The high-amplitude post-flutter frequencies listed in Table IX indicate this trend for the cracked blades (blades 1, 2, and 3).

TABLE IX

FREQUENCIES OF DAMAGED BLADES

Blade	Low-Amplitude Pre-Flutter	Low-Amplitude Post-Flutter	High-Amplitude Post-Flutter
1	359.3 Hz	308.1 Hz	288.3 Hz
2	359.0	349.4	333.1
3	360.0	287.7	252.0
4	359.7	359.1	359.0
5	346.7 (untuned)	328.9	329.1

Assuming the cracked blade is, in fact, a nonlinear stiffness system, and further assuming the blade to be describable as a lumped spring-mass oscillator, then an appropriate model describing the blade motion is given by Duffing's equation (Reference 9):

$$\ddot{x} + \gamma \dot{x} + (\alpha x - \beta x^3) = F\cos\omega t,$$

where the negative sign is used with the nonlinear term to represent the observed soft-spring behavior of the blade (i.e., frequency decreasing with increasing amplitude). The corresponding frequency response curve for the nonlinear problem is sketched in Figure 26 and is described in detail in Reference 9. The frequency, f_o, shown in this figure denotes the natural frequency at small amplitudes. It is clearly seen that as the amplitude of the motion is increased, the resonant frequency value decreases. It is also important to note that for high enough amplitudes, the response curve folds over itself causing it to have two vertical tangents. This behavior of the frequency response represents an important physical characteristic of nonlinear spring systems in that it shows amplitude jumps occurring at two different values of frequency.

In relation to this, it is appropriate at this point to describe a separate bench test that was performed on blade 3 (which was the most severely damaged). This was done to prove that Duffing's equation is the correct approximate model for explaining the observed decrease in frequency as the amplitude of the cracked blades increases. This test was carried out using a small, but finite, constant amplitude drive force which caused the leading edge of the blade to oscillate with a peak amplitude of approximately 0.05 inches. The signal generator was set at a frequency slightly above 288 Hz (the post-experiment small-amplitude frequency response of blade 3), and the frequency was slowly lowered. As the frequency became smaller, the response amplitude increased until the frequency reached 276 Hz at which point the amplitude suddenly dropped to only 12 percent of its peak value. The experiment was repeated, but this time from below 276 Hz. As the frequency was slowly increased from about 10 percent peak amplitude, the amplitude grew until it reached 40 percent of the peak value recorded at 276 Hz. At this point (f = 281.5 Hz), the amplitude jumped to 74 percent of peak value. This jump phenomenon agrees with what is physically indicated in Figure 26, which traces the hysteresis loop of blade 3 where the jumps in amplitude occur at points of vertical tangency. It is seen in Figure 26 that the magnitude of the jump from point 2 to point 3 is greater than the magnitude of the amplitude jump from point 5 to point 6. This behavior of the soft-spring response curve agrees with the experimental observations just described, where the jump at 276 Hz corresponds to the drop in amplitude from point 2 to point 3 and the jump at 281.5 Hz corresponds to the sudden increase in amplitude from point 5 to point 6. This result lends confidence in the choice of Duffing's equation as a model of the damaged blade response.

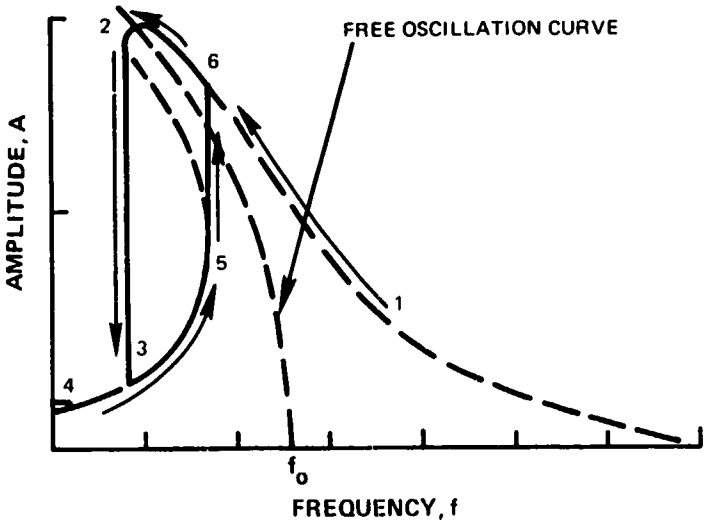

FIGURE 26 Nonlinear Frequency Response

With this additional confidence in the model, it is possible to estimate the frequency variation with amplitude. First, an expression of the free oscillation curve is obtained from the first order perturbation solution of Duffing's equation (Reference 9). Upon assuming that β (nonlinear stiffness coefficient) is constant for all amplitudes, the following expression for frequency is obtained directly

$$f = f_o \sqrt{1 - \left[1 - \left(\frac{f_1}{f_o}\right)^2\right] \left(\frac{A}{A_1}\right)^2} \qquad (1)$$

where f_o is the small-amplitude natural frequency, and f_1 and A_1 are values of frequency response and amplitude, respectively, for one test case. (It is interesting to note that this equation is a first quadrant trace of an ellipse.) From the bench test experiment just described for blade 3, f_o = 288 Hz, f_1 = 276 Hz, and the leading edge amplitude A_1 = 0.05 inches. Therefore,

$$f \cong 288 \sqrt{1 - 32.64A^2} \qquad (2)$$

for blade 3 frequency response, where A represents leading edge displacement in inches. It was noted in this report that during the flutter test, blade 3 was observed to oscillate with a leading edge amplitude deflection of approximately 0.1 inches at M = 1.65. At this amplitude the corresponding frequency is f = 236 Hz, which is reasonably close to both the actual measured value of the primary response of 245 Hz in the tunnel, and 252 Hz measured for the high-amplitude excitation bench test (Table IX). Furthermore, if the amplitude A is assumed to be 0.12 inches the predicted frequency would be 209 Hz which shows the extreme sensitivity of frequency response with small changes in amplitude, and may help to explain the emergence of 190 Hz as a secondary system frequency (cf. Appendix VII).

APPENDIX VII

SPECTRAL ANALYSIS PROCEDURES

The time history of the blade stress response was analyzed by spectral techniques. As stated in the main text of this report, a single time history was taken of the flutter condition which was later analyzed over several selected regions of interest, each of which is referred to as a point. The acquisition rate of the WISARD was 7500 samples/sec/channel at the original recording speed of 7.5 inches/sec. Hence, for a flutter frequency of 250 Hz this yielded 30 samples/cycle which was sufficient for an accurate analysis.

The spectral analysis for each point consisted of obtaining power spectra (or auto-correlations) for each blade and cross-power spectra (or cross-correlations) for each blade pair. The power spectrum yielded the square of the amplitude of the response versus frequency, and revealed the resonant peaks for each blade. The cross-power spectrum was useful for obtaining the interblade phase angle between different pairs of blades. Both of these results were used in the main text to describe the phenomena associated with the flutter test data.

Two samples of data are discussed herein to illustrate the characteristics of the spectral techniques. Point 1 was described in the text as a condition in which all blades oscillated at a primary frequency of f = 245 Hz. The time history was shown in the upper panel of Figure 9 in the main text.

Some sample power spectral plots for this point are shown in Figures 27 through 29 Figures 27 and 28 contain the autocorrelations of blades 2 and 3, and Figure 29 contains the cross correlation of blades 2 and 3, respectively, each of which are plotted versus frequency. These particular blades were chosen because blade 2 generally showed a strong tendency to oscillate only at 245 Hz while blade 3 was capable of oscillating at both 245 Hz and 190 Hz. The ordinate in each plot is the square of the response amplitude, plotted on a logarithmic scale such that each unit represents an order of magnitude change. Figure 27 shows that blade 2 fluttered primarily at 245 Hz, and that its response at 190 Hz was nearly 4 orders of magnitude lower. A third harmonic peak at approximately 750 Hz was slightly more than 2 orders of magnitude below the primary peak. Figure 28 for blade 3 indicates a primary peak at approximately 245 Hz with a secondary peak 1 order of magnitude smaller at approximately 190 Hz and a somewhat smaller peak at 225 Hz. The peak at 760 Hz probably represents the fourth harmonic of the 190 Hz response and the minor peak at 490 Hz is the second harmonic of the 245 Hz response. The peak at 430 Hz is not a harmonic of any of the lower frequencies, and it is possible that it represents excitation in some mode other than the primary flutter mode. The cross correlation of blades 2 and 3 is found in Figure 29. The strong primary peak at 245 Hz, the minor peak at 225 Hz, and the absence of any other peaks within 2 orders of magnitude of the primary is a further indication of the concentration of energy in the higher frequency mode. The autocorrelation plots in Figures 27 and 28 also yielded the harmonic amplitude ratios plotted in Figure 9 for blades 2 and 3. These were obtained from the square root of the ratio of the amplitudes at 245 Hz and 190 Hz.

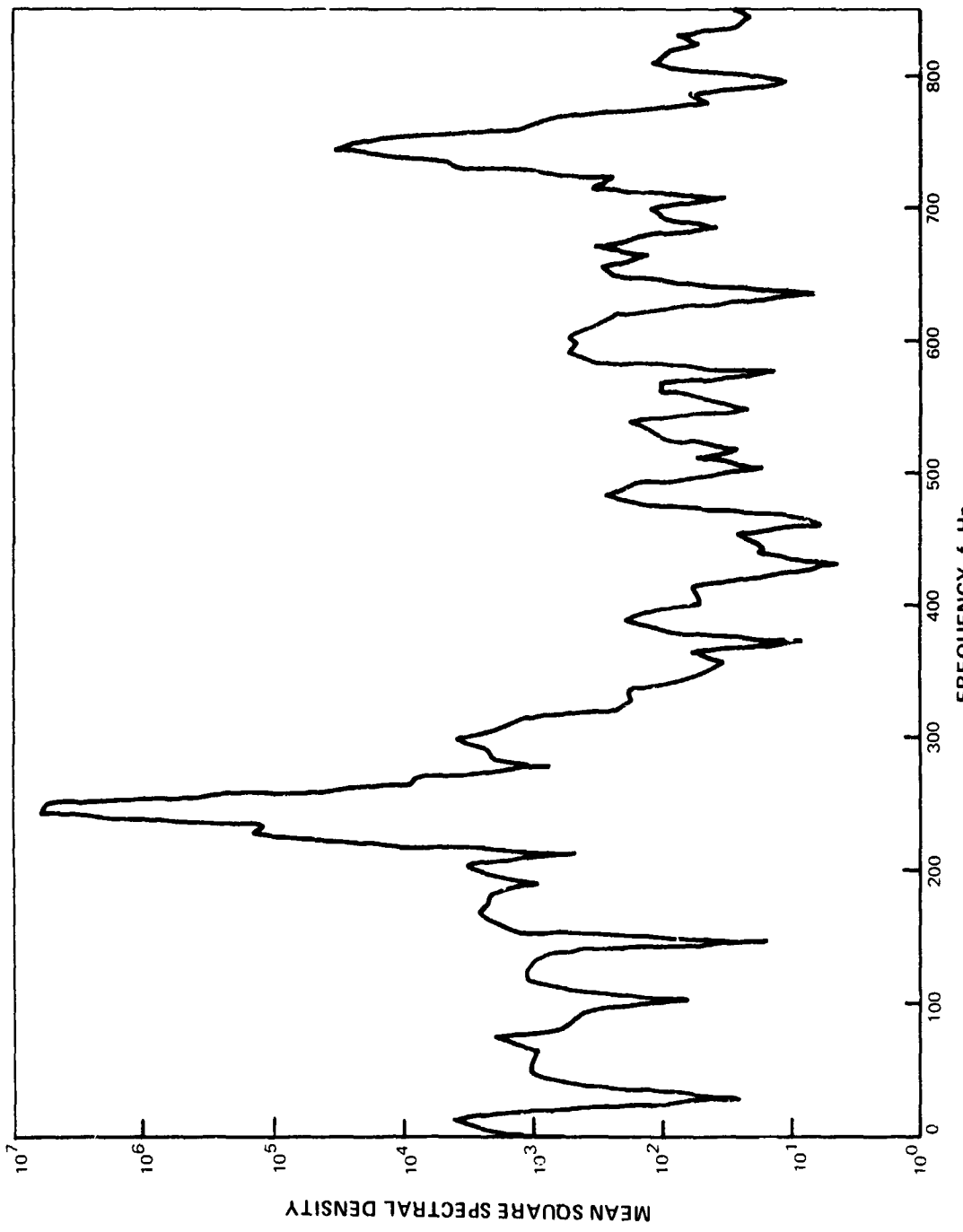

FIGURE 27 Autocorrelation of Blade 2 at Point 1

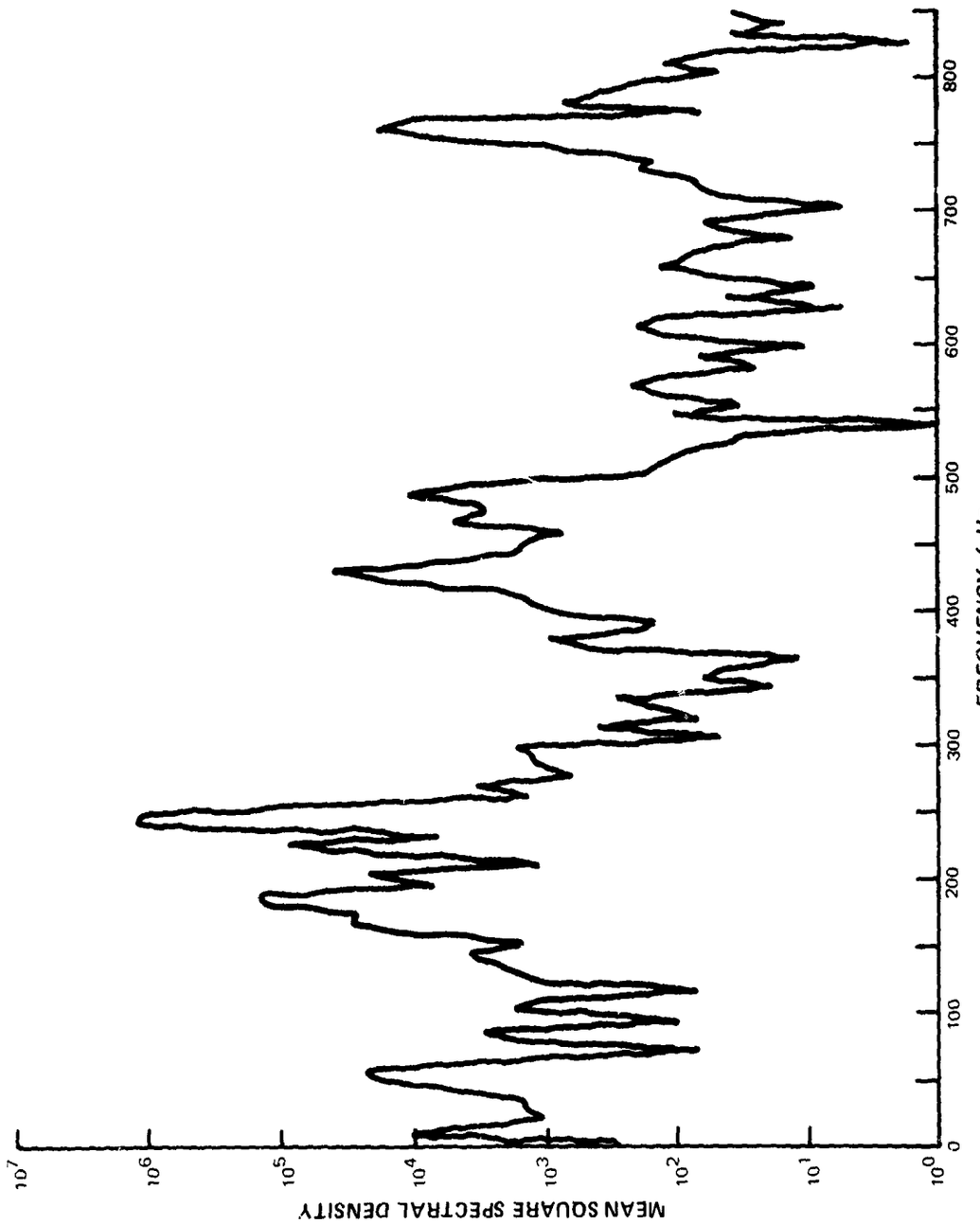

FIGURE 28 Autocorrelation of Blade 3 at Point 1

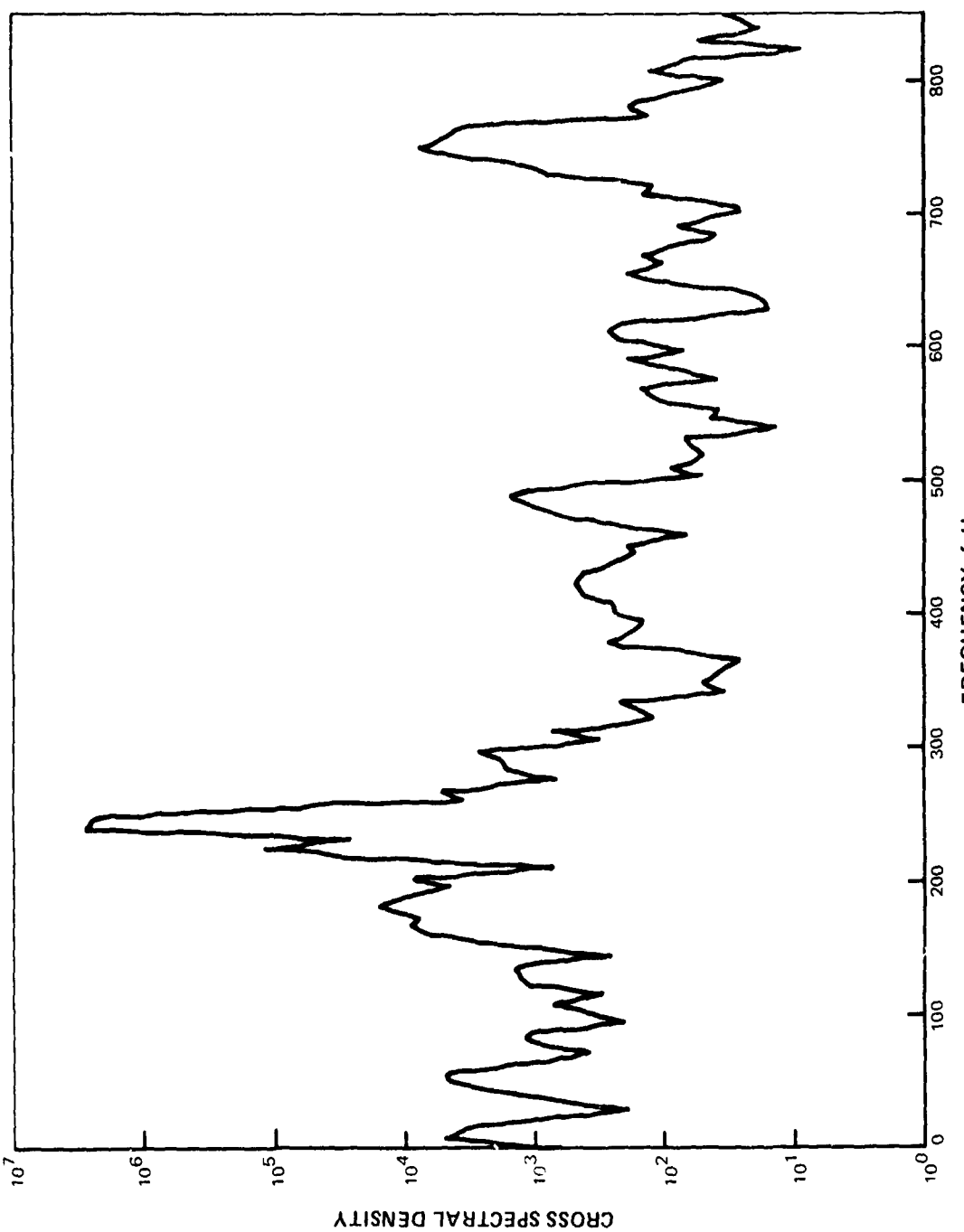

FIGURE 29 Cross-Correlation of Blades 2 and 3 a: Point 1

Point 2 was described in the text as a condition in which blade 2 oscillated primarily at the higher frequency, and blade 3 oscillated with a strong 190 Hz frequency component. In Figure 30, for blade 2, the primary peak is still at 245 Hz but a secondary peak is clearly evident at 190 Hz, approximately 2 orders of magnitude smaller. (Note that the square root of 10^2, which is the ratio of the square of the amplitudes, yields a harmonic amplitude ratio of 10, which is approximately the value plotted for blade 2 in Figure 10.) The primary peak for blade 3 in this instance is at 190 Hz as shown in Figure 31. The peak at 245 Hz is roughly 1/3 order of magnitude smaller, and all other peaks are even smaller. As seen in the time history of Figure 10, the frequency of blade 3 abruptly changed several times during this part of the record between 190 Hz and 245 Hz. The cross-correlation plot in Figure 32 shows that although the major peak still occurs at 245 Hz, a significant peak is also located at 190 Hz, indicative of a sharing of the energy between both blades at both frequencies.

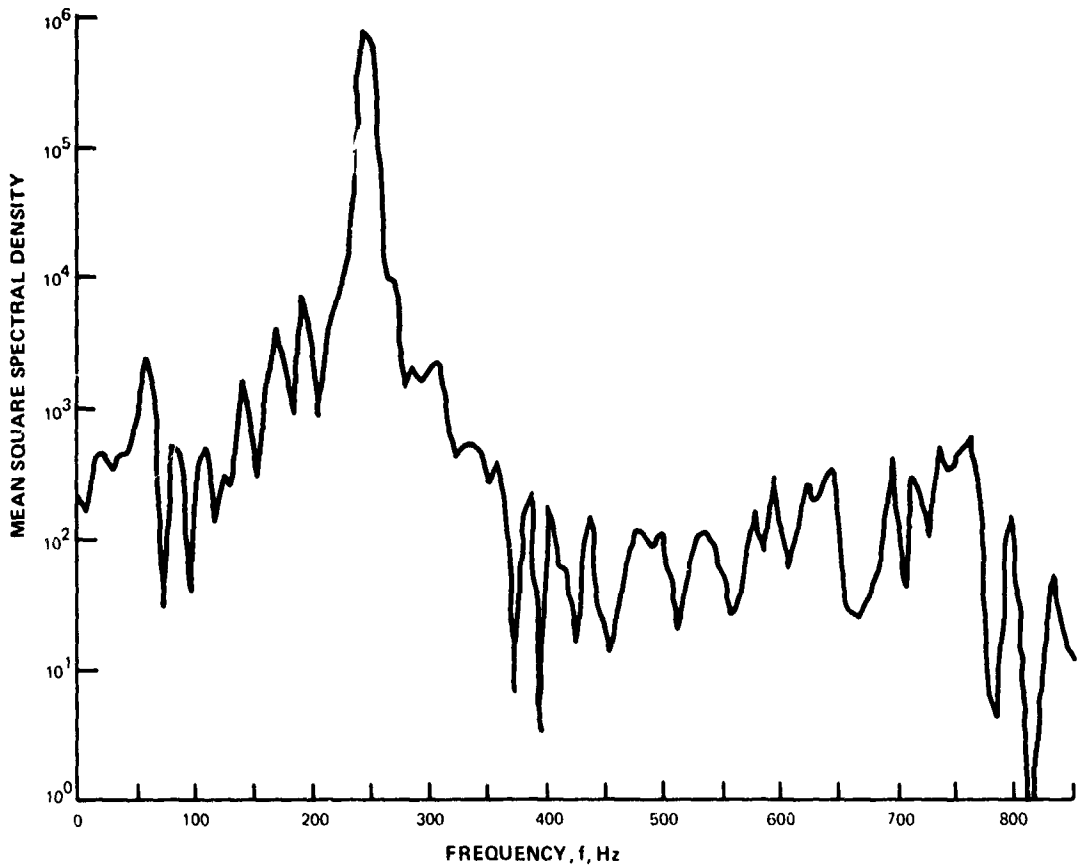

FIGURE 30 Autocorrelation of Blade 2 at Point 2

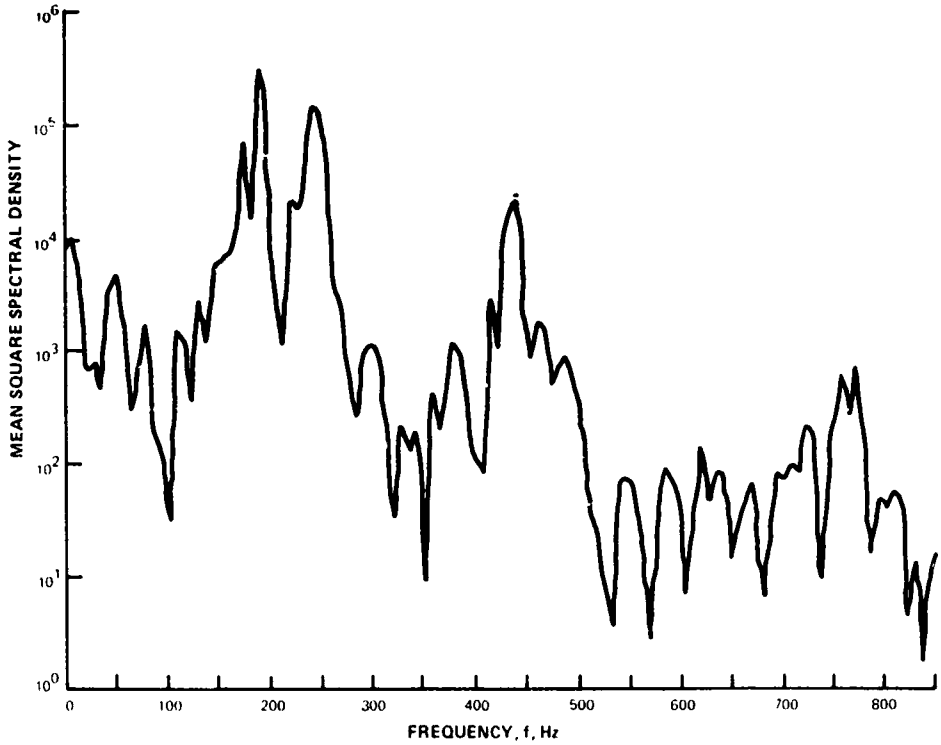

FIGURE 31 Autocorrelation of Blade 3 at Point 2

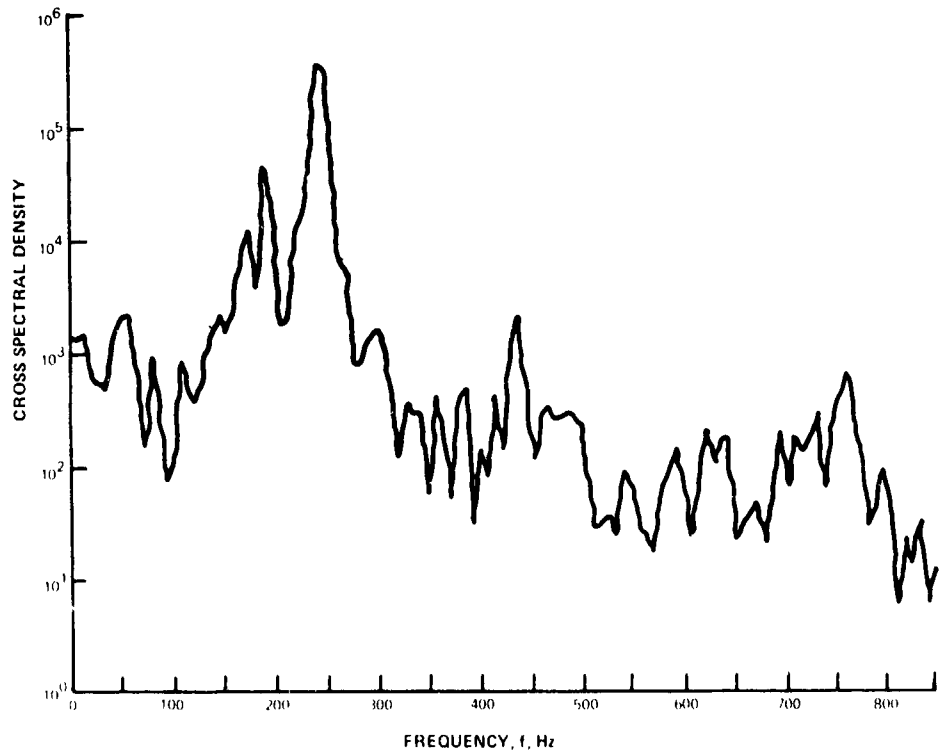

FIGURE 32 Cross-Correlation of Blades 2 and 3 at Point 2